NAVAL POSTGRADUATE SCHOOL
Monterey, California

REDESIGN OF THE LOW SPEED THREE STAGE

AXIAL FLOW COMPRESSOR TEST FACILITY

by

M. H. Vavra
P. F. Pucci
W. Schlachter

December 1973

Approved for public release, distribution unlimited

NAVAL POSTGRADUATE SCHOOL
Monterey, California 93940

Rear Admiral M. B. Freeman
Superintendent

J. R. Borsting
Provost

ABSTRACT:

A flow configuration of an existing low-speed, axial flow compressor test facility at the Turbopropulsion Laboratory, Naval Postgraduate School, Monterey, California, was redesigned in order to improve compressor inlet velocity distribution, improve mass flow measurement, and increase the power input. The design of the new configuration, consisting of an inlet nozzle, ducting, throttling device upstream of the compressor, and a diffusor downstream of it, is reported. The redesign is based on using the existing free-vortex type and solid-body type bladings, and the newly designed symmetrical blading.

This study has been supported by:

Naval Air Systems Command, Code 310
AIRTASK No. A310 310A/186A/3R02403001

CONTENTS

LIST OF TABLES

LIST OF FIGURES

INTRODUCTION

The three-stage, axial flow compressor test rig of the Turbomachinery Laboratory of the Department of Aeronautics, Naval Postgraduate School, Monterey, California, was acquired from the California Institute of Technology, Pasadena, California. It was used in the acquired configuration for several test programs until a recent experimental program to determine the influence of blade loading on tip clearance effects was begun which required the redesign of the facility.
The object of this report is to present some of the reasons that led to the decision to redesign, and to present a review of the design criteria.

DECISION TO REDESIGN

The original configuration presented several limitations. See Figure 1. In particular, the flow rate was controlled by a throttle at the compressor discharge, which caused asymmetric velocity distributions leaving the compressor. Asymmetric velocity profiles were also detected at the entrance portion of the inlet duct. Since mass flow rate is determined by the integration of the entrance velocity profile, this results in an uncertainty in the mass flow rate. Also, interstage measurements are restricted to a small angle of the periphery. A uniform velocity profile ahead of the compressor is required to assume axial symmetry and to apply these measurements to the entire periphery for overall performance determinations. In the investigation of tip clearance losses, an accurate determination of the mass

flow rate is essential, and therefore an alternate to the original design was required.

DESIGN CRITERIA

The facility design was changed to a system in which the mass flow rate is controlled by a throttling device located in the inlet duct to the compressor. The overall requirements of the inlet section are to

(a) provide an axisymmetric flow as uniform as possible ahead of the compressor

(b) provide the means for an accurate determination of the mass flow rate

(c) allow an easy adjustment of the mass flow rate

(d) minimize pressure losses at the zero throttling position so that as high an operating mass flow rate range as possible may be achieved.

Requirements (b) and (d) are contradictory. Using an inlet nozzle for the flow measurement requires sufficiently large pressure drops for accuracy, whereas as low a pressure drop as possible is desired to obtain the maximum flow rates.

The component arrangement is shown in Figure 2. The required inlet sections include the inlet nozzle, the throttling device and the required ducting between the inlet nozzle and throttle and between the throttle and the compressor. The change in design also includes the addition of a diffusor section immediately downstream of the compressor discharging to atmosphere, a new drive motor with increased

horsepower capability, and a torque meter on the compressor drive shaft.

With higher horsepower available, higher pressure ratios are attainable and hence an improvement in the measuring accuracy is possible. In the following, the design and specification of the components cited above will be discussed in detail.

OPERATING RANGE

The operating range of the compressor was determined by Vavra (1) in the design of the symmetrical blading to be used in one, two, and three stages. The compressor speed for each of these configurations is based on the absorption of 135 hp at the design point. The drive motor is rated at 150 hp, 1180 rpm, 440v/3Ø, 190 amps continuous operation, which allows for operation at overload conditions. A fixed V-belt pulley drive is used to obtain the desired compressor speeds of 2290, 1818, and 1588 rpm (1).

The off-design performance of the sym metrical blading was then determined. Several simplifying assumptions were made:

1. The performance of the stage element at the blade mean radius, R_m, is representative of the whole stage.

2. The axial components of the absolute velocity ahead of and after the rotor blades at the mean radius, R_m, are set equal to each other with a magnitude equal to the average of the original components, i.e., $V_a = 1/2 \left(V_{a1} + V_{a2} \right)_{R_m}$.

3. The energy input to the rotor stage at the design point, as indicated by the magnitude of the change in the tangential component of the absolute velocity, ΔV_u, is set equal to the value obtained by Vavra (1).

4. The radial shift of the streamlines can be ignored.

5. The stator discharge angle remains constant at a given compressor rotational speed for all mass flow rates within the range of interest.

6. Changes in the rotor discharge angle are calculated assuming the two-dimensional cascade data of reference (2) Chapter VI.

7. The losses in the rotor and stator are equal.

8. The flow conditions established for a single stage are repeated for multi-stage operation.

The symmetry of the blading, together with assumptions 2 and 3 above, modifies the original velocity triangle from that of Figure 3(a) to that of Figure 3(b). Note that magnitudes of all angles and velocity vectors except Δv_u and $R_m\omega$ will be changed slightly during this operation.

A summary of corresponding values at the design point from the original computations of Vavra (1) and the modified values resulting from the above assumptions is given in Table I.

The procedure for obtaining the modified velocity triangle from the original design point velocity triangle is given in Appendix A.

WORK REQUIRED AT OFF-DESIGN CONDITIONS

The off-design conditions investigated are those operating points at a specified compressor rotational speed with differing mass flow rates.

Symbolically, these conditions will be represented by affixing the superscript prime to the variable under consideration, e.g., V_a' . Physically, the mass flow rate will be varied by throttling. Analytically, the mass flow rate is varied by changes in the axial component of the absolute velocity, V_a' . From Figure 4, note that with a fixed direction of the absolute inlet velocity, V_1 , that is, a constant inlet guide vane discharge angle, α_1 , (see assumption 5 above), and a fixed rotational speed, ω , changes in the axial component, V_a' , are reflected in changes in the direction of the relative inlet velocity, W_1 , that is, in the angle β_1 . It is somewhat less convenient to vary β_1 in the analysis than the axial component, V_a' , so that this means will be used. The interrelationship between the significant geometric and flow angles is shown in Figure 5. In particular, note that for a given blade geometry, that is, with a given camber angle, $\emptyset$, and a given stagger angle, γ , the relative flow angles β_1' and β_2' are directly related to the incidence angle, i' , and the deviation angle, δ' , respectively. Thus, by selecting a β_1' for an off-design point analysis, the incidence angle, i' , is readily computed.

The sensitivity of the deviation angle to changes in the incidence angle has been reported by Lieblein (2) for experimental flow in two-dimensional cascades. In the flow regime of minimum loss, this dependence is given by

$$\delta' = \delta_{ref} + (i' - i_{ref}) \left(\frac{d\delta}{di} \right)_{ref} \qquad \text{EQN (1)}$$

where the slope, $\left(\frac{d\delta}{di}\right)_{ref}$ is a function of the solidity, σ , and the relative flow angle, β_1 . The reference values chosen are the design point values from Vavra (1), which were selected for minimum loss based on this same reference.

With this value of the deviation angle, the flow deflection angle becomes (see Figure 5)

$$\Delta\beta' = \beta_1' - \beta_2' = \phi + i' - \delta' \qquad \text{EQN (2)}$$

This value of the flow deflection angle is related to the original value calculated at the design point. The flow deflection angle for the modified velocity triangle at this off-design condition, $\Delta\beta'_{mod}$, is assumed to be in the same ratio to the flow deflection angle obtained from the original values, $\Delta\beta'$, as the ratio of the flow deflection angle for the modified velocity triangle at the design point, $\Delta\beta_{mod}$, is to the flow deflection angle, $\Delta\beta$, from the original design point data (1), i.e.,

$$\Delta\beta'_{modified} = \Delta\beta' \cdot \frac{\Delta\beta_{modified}}{\Delta\beta} \qquad \text{EQN (3)}$$

Thus, the relative flow direction at the rotor exit

$$\Delta\beta'_{2_{modified}} = \beta'_{1_{modified}} - \Delta\beta'_{modified} \qquad \text{EQN (4)}$$

The non-dimensional form of the velocities is obtained by referring them to the rotor peripheral speed at the mean radius, $U = R_m \cdot \omega$. These will be designated by the superscript asterisk, e.g.,

$$V_a^* = \frac{V_a}{U} = \frac{V_a}{R_m \cdot \omega}$$

The modified velocity triangle is shown in Figure 6.

At large positive incidence angles, the flow separation on the suction side of the blades causes the deviation angles, δ , and the relative flow deflection angles, $\Delta\beta$, to be significantly different than those values calculated above in Equations (3) and (4). Howell (3) indicates the magnitude of this difference and it has been incorporated into the off-design calculations at incidence angles greater than +2° (corresponding to relative inlet flow angles, β_1 , greater than 45°.)

A plot of the resulting calculated relative turning angle ratio, $\frac{\Delta\beta'}{\Delta\beta}$ as a function of the dimensionless incidence angle, $\frac{(i' - i)}{\Delta\beta}$ is shown in Figure 7.

From Figure 6, note that

$$V_a^{*'} = \frac{1}{\tan \alpha_1 + \tan \beta_1'} \qquad \text{EQN (5)}$$

and that the increase in the tangential component of the absolute velocity, $\Delta V_u^{*'}$, is given by

$$\Delta V_u^{*'} = V_{u2}^{*'} - V_{u1}^{*'} = 1 - V_a^{*'}(\tan \alpha_1 + \tan \beta_1') \qquad \text{EQN (6)}$$

Substituting the expression for $V_a^{*'}$ from EQN (5) into EQN (6) results in

$$\Delta V_u^{*'} = \frac{\tan \beta_1' - \tan \beta_2'}{\tan \alpha_1 + \tan \beta_1'} \qquad \text{EQN (7)}$$

The losses attributable to operation at off-design incidence angles and the range of operation as defined by the stall limits has been estimated using the results of Howell (3) and Lieblein (2).

Lieblein found that an equivalent diffusion factor, D_{eq}' can be related to the off-design flow angles as follows:

$$D_{eq}' = \frac{\cos \beta_2'}{\cos \beta_1'} \left[1.12 + a(i' - i)^{1.43} + 0.61 \frac{\cos^2 \beta_1'}{\sigma} (\tan \beta_1' - \tan \beta_2') \right] \quad \text{EQN}$$

where a = 0.007 for the C-4 circular arc blades. He found that blade stall can occur at positive incidence angles for which the equivalent diffusion factor, D_{eq}' , is greater than 2.0. Therefore, using this criterion, the positive incidence angle where stall is likely to occur, i_{st}' , can be determined. It was found that the ratio, $\frac{i_{st}' - i}{\Delta\beta}$, is near 0.45. This is also the region where the turning angle, $\Delta\beta$, departs from its lower incidence angle behavior. (See Figure 7.) Using this value for the positive stall limit together with the reference incidence angle established a half range of operation which then sets the negative stall limit at a value $\frac{i_{st}' - i}{\Delta\beta} = - 0.45$. Howell (3) found that the magnitude of the loss coefficient near stall is twice the minimum value. Combining these two criteria for stall establishes the magnitudes of the loss coefficients and incidence angles at stall. Further, it assumes that the variation of the loss coefficient with incidence angle is similar to the observed values by Lieblein (2) . This variation, in normalized form, is shown in Figure 8, where $\bar{Y}$ is the minimum loss coefficient, and Y' the off-design loss coefficient.

PRESSURE RISE ACROSS A STAGE

The total pressure loss in a rotor is customarily defined as a fraction

of the inlet relative velocity head, that is,

$$\Delta P_{t_R} = Y_R \tfrac{1}{2} \rho w_{in}^2$$

and similarly for a stator

$$\Delta P_{t_S} = Y_S \tfrac{1}{2} \rho V_{in}^2$$

where Y_R and Y_S are defined as the loss coefficients for the rotor and stator respectively. It is assumed for this analysis that the rotor and stator loss coefficients are equal at the design point, that is, $Y_R = Y_S = \bar{Y}$.

For the separate discussion of the compressor, establish the position locations as follows:

Section 1 : rotor inlet

Section 2 : rotor exit and stator inlet

Section 3 : stator exit,

as indicated in Figure 9.

The overall stage efficiency, η_t , defined as the ratio of the total pressure rise to the theoretical maximum total pressure rise, becomes

$$\eta_t = \frac{P_{t_3} - P_{t_1}}{(P_{t_3} - P_{t_1})_{theo.}} = \frac{P_{t_3} - P_{t_1}}{\rho R_m \omega (\Delta V_u)} \qquad \text{EQN (9)}$$

At the design-point $\bar{\eta}_t = 1 - \dfrac{\bar{Y}\,(w_1^{*2} + V_2^{*2})}{2x}$ EQN (9a)

and at off-design $\bar{\eta}_t' = 1 - \dfrac{\bar{Y}'(w_1^{*'2} + V_2^{*'2})}{2x'}$ EQN (9b)

Combining the dimensionless pressure rise, $\bar{\pi}_{t_3}$, defined as

$$\bar{\pi}_{t_3}' = \frac{\bar{P}_{t_3}' - \bar{P}_{t_1}'}{\rho \omega^2 R_m^2} \qquad \text{EQN (10)}$$

with the definition of the stage efficiency yields

$$\pi'_{t_3} = \bar{\eta}'_t \cdot X' \qquad \text{EQN (11)}$$

Therefore, from Equations (9b), (10), and (11), the average total pressure at the stage exit can be obtained in terms of the average stage inlet total pressure.

For a multistage compressor, it is assumed that conditions repeat from stage to stage, such that for Z stages, the overall total pressure rise is given by

$$\bar{\pi}'_t = Z \cdot \bar{\eta}'_t X' \qquad \text{EQN (12)}$$

Using the above equations, the total pressure ratio, $\bar{\pi}'_{t_3}$, at the design point is slightly greater than that obtained by Vavra (1), $\bar{\pi}_t$, which is an integrated average of the variation across the blade height and obviously a better solution than the mean value obtained above by using the modified velocity triangle. Thus, the total pressure ratio at the design point obtained by Vavra (1) is used. Assuming that the off-design total pressure ratios calculated by the above modified velocity triangle method can be improved by stating the ratio of improved to calculated total pressure ratios at off-design is equal to the ratio of that obtained by Vavra to the calculated value at design. Thus, the improved (or corrected) off-design total pressure ratio becomes

$$\bar{\pi}'_{t_3}{}_{\text{imp.}} = \bar{\pi}'_{3}{}_{\text{mod.}} \cdot \left[\frac{\bar{\pi}_{t_3}{}_{\text{Ref. (1)}}}{\bar{\pi}_{t_3}{}_{\text{mod.}}} \right]_{\text{design pt.}} \qquad \text{EQN (13)}$$

For incompressible flow, the off-design power input, L' , is related to the power input at the design point, L , at the same rotational speed by

$$\frac{L'}{L} = \frac{V^{*\prime}_{a} \; X'}{V^{*}_{a} \; X} \qquad \text{EQN (14)}$$

The corresponding calculations are indicated in TABLE 2. and in Figure 10.

The expected mass flow rates range can be determined from the design point values given by Vavra (1) and the mass flow functions at the assumed stall limits interpolated from Table 2. A summary of the results is tabulated below:

		1 Stage	2 Stages	3 Stages
Speed	RPM	2290.	1818.	1598.
Design Volume Flow Rate	ft^3/sec	1034.	820.	718.
Design Mass Flow Rate	slugs/sec	2.452	1.944	1.708
Maximum Mass Flow Rate	slugs/sec	3.059	2.426	2.131
Minimum Mass Flow Rate	slugs/sec	1.943	1.541	1.353

FREE-VORTEX AND SOLID-BODY BLADING

The performance of the free-vortex type and the solid-body type blading has been measured in previous tests. The expected operating range using these bladings at the desired compressor speeds for the symmetrical blading was checked for compatibility with the redesigned facility. Performance maps of the free-vortex and solid-body bladings are presented in Figure 5 of Reference (4) and Figure 46 in Part 2 of Reference (5).

The rotor tip speed, ωR_t , was used in the correlating dimensionless parameters, $\bar{\psi}$, $\bar{\psi}'$, and $\bar{\phi}$. The data presented are put into the form used in this report by changing the reference speed from the rotor tip speed to the speed at the mean blade radius, R_m . In addition, the symbology has been changed to conform with this report. The necessary conversions are summarized as follows:

Flow coefficients: $$\varphi = \bar{V}_a^* = \frac{V_a}{\omega R_m} = \phi \frac{R_t}{R_m} \qquad \text{EQN (15)}$$

Work coefficients: $$X = \frac{\bar{\Delta H}}{(\omega R_m)^2} = \frac{\bar{\psi}}{2} \left(\frac{R_t}{R_m} \right)^2 \qquad \text{EQN (16)}$$

where $\bar{\Delta H}$ is the increase in the total enthalpy per stage.

Head coefficients: $$\bar{\pi}_{t_3} = \frac{P_{t_3} - P_{t_1}}{\rho (\omega R_m)^2} = \frac{\bar{\psi}}{2} \left(\frac{R_t}{R_m} \right)^2 \qquad \text{EQN (17)}$$

Also, the average total-to-total stage efficiencies are related by

$$\bar{\eta}_t = \frac{\bar{\pi}_t}{X} = \frac{\bar{\psi}'}{\psi} \qquad \text{EQN (18)}$$

Figure 11 presents the off-design performance of three stages of free-vortex type blading. Included on the figure is the pressure ratio of one stage of solid-body type blading. The behavior of the solid-body type blading is very nearly that of the free-vortex type blading, thus the off-design performance of the free-vortex type blading will be assumed to represent the behavior of both types. The horsepower, L , required at the design speeds are first determined to compare with the available horsepower of the new drive system.

$$L = \pi (R_t^2 - R_h^2) \rho \varphi z \bar{\pi}_{t_3} (\omega R_m)^3 \frac{1}{\bar{\eta}_t} \qquad \text{EQN (19)}$$

For the redesigned facility, R_t = 18.0 in., R_h = 10.6 in., and R_m = 14.4 in. Also, φ = 0.5625 (ϕ = 0.45) at design conditions, and $\rho = 2.731 \times 10^{-3}$ slugs/ft^3. From Figure 11,

for Z = 1 : $\overline{\pi}_{t_3}$ = 0.258 and $\overline{\eta}_t$ = 0.897; and

for Z = 3 : $\overline{\pi}_{t_3}$ = 0.258 and $\overline{\eta}_t$ = 0.85.

Assume for two stage operation that $\overline{\pi}_{t_3}$ = 0.258 and that $\overline{\eta}_t$ is the arithmetic average of $\overline{\eta}_t$ for one and three stages, i.e.,

$$\overline{\eta}_t = 1/2 \; (\; 0.897 + 0.85 \;) = 0.873$$

The power required by the free-vortex type and the solid-body type bladings at the three rotational speeds fixed by the symmetrical blading design for one, two, and three stages operation is summarized in the table below:

DESIGN POINT HORSEPOWER REQUIRED BY THE FREE-VORTEX AND SOLID-BODY TYPE BLADINGS

Stages			Horsepower, L		
Z	$\overline{\pi}_{t_3}$	$\overline{\eta}_t$	N = 1588 rpm,	1818 rpm,	2290 rpm
1	0.258	0.897	25.1	37.6	75.2
2	0.258	0.873	51.5	77.3	154.5
3	0.258	0.850	79.4	119.1	238.1

From the above table, operation at 2290 rpm with two or three stages is not possible with the 150 hp motor. In addition, a conservative extrapolation for three stage operation at the minimum flow stall limit (φ = .30) is obtained from that of one stage. This off-design

horsepower is approximately 1.8 times the design horsepower. Thus, for three stage operation at 1818 rpm, the off-design required horsepower, $L' = L \times \frac{L'}{L} = 119.1 \times 1.8 = 214.4$ hp. This precludes operation at this off-design limit.

The expected mass flow rates range can be deduced from the data in Reference (1). The flow function of Reference (2), $\bar{\phi}$, is

$$\bar{\phi} = \frac{Q}{\omega_R R_t \pi (R_t^2 - R_h^2)} \qquad \text{EQN (20)}$$

The flow function, φ, of this report is related to $\bar{\phi}$ as follows:

$$\varphi = \bar{\phi} \frac{R_t}{R_m} \qquad \text{EQN (21)}$$

A summary of the results is tabulated below:

MASS FLOW RATES OF THE FREE-VORTEX AND SOLID BODY TYPE BLADINGS

Stages		1			2		
Speed	rpm	2290	1818	1588	1818	1588	1
Design Volume Flow Rate	ft^3/sec	732.3	581.4	564.2	581.4	507.8	50
Design Mass Flow Rate	slugs/sec	1.736	1.378	1.204	1.378	1.204	1.
Minimum Mass Flow Rate	slugs/sec	0.965	0.766	0.669	0.884*	0.748*	0.
Maximum Mass Flow Rate	slugs/sec	1.929	1.532	1.3378	1.720*	1.405*	1.

* Results for two stages are estimated as the average of the flow rates at one and three stages.

INLET NOZZLE

Two requirements of the inlet nozzle are to provide for a sufficiently large pressure drop from the atmospheric pressure, P_a, to the nozzle throat static pressure, P_1', for reasonable flow measurement accuracy, along with a minimum distortion of the velocity profile.

For the isentropic flow of a perfect gas with constant specific heats, the mass flow rate through the inlet nozzle is given by

$$\dot{m}_{is.} = \pi R_N^2 \left[\rho_a \cdot 2 (P_a - P_1') \right]^{\frac{1}{2}} \left[1 - \frac{3}{4\gamma} \left(\frac{P_a - P_1'}{P_a} \right) \right] \quad \text{EQN (22)}$$

where the higher order terms of the nozzle pressure ratio expansion has been neglected. For a pressure ratio, $\frac{P_a - P_1'}{P_a} = 0.06$ (corresponding to a pressure drop, $P_a - P_1'$, of approximately 25.0 inches of water), results in an error of less than 0.05%.

The pressure drop for the expected minimum flow rate was calculated using Equation (22) above with $P_a = 14.696$ psia, $T_a = 59°F$, $\gamma = 1.40$, and setting $R_N = R_t$. The minimum mass flow rate of approximately 0.67 slugs/second occurs for one stage operation of the free-vortex type blading at 1588 rpm. The resulting pressure drop of less than 0.35 inches of water is too small a pressure drop for accurate measurements of mass flow rate. In order to increase this pressure drop, the nozzle throat area must be reduced. The variation of pressure drop with mass flow rate for various throat diameters was calculated and the results shown in Figure 12. Also indicated on

the figure are the expected mass flow rate ranges of the symmetrical, free-vortex and solid-body type bladings. Selection of the design radius ratio, $\beta = \frac{R_N}{R_t}$, depends on the criterion set for a minimum acceptable pressure drop. If a pressure drop of 2.0 inches of water is selected as a minimum, the largest β permissible for the minimum mass flow rate of approximately 0.67 slugs/second is approximately 0.65. At the minimum mass flow rate with two stages of free-vortex or solid-body type blading, a β of 0.7 is required. For three stage operation, the pressure drop is slightly greater than the desired 2.0 inches of water at minimum mass flow if a β of 0.7 is chosen. However, to restrict the number of inlet nozzles to be made, only one β less than unity is desired. Use of $\beta = 0.7$ for one stage of operation is satisfactory for most of the flow rate range. The compromise made is that there is a relatively large pressure drop of approximately 12.5 inches of water at the maximum mass flow rate. Whether this is acceptable or not remains to be determined in the overall pressure compatibility of the system.

For the symmetric type blading, the minimum mass flow rate obtained during three stage operation requires a β of 0.9 or less. Hence, a $\beta = 0.7$ will be acceptable if the higher pressure drop is compatible. For operation with one or two stages, a $\beta = 1.0$ is satisfactory. Therefore, the design criteria for nozzle sizes are as tabulated below:

Operational Mode		Operational Mode	
Free-Vortex or Solid-Body Type Blading	β	Symmetric Type Blading	β
One Stage	0.7	One Stage	1.0
Two Stages	0.7	Two Stages	1.0
Three Stages	0.7	Three Stages	0.7

These selections are to be checked for overall pressure compatibility.

An inlet nozzle contour with a gradually decreasing curvature in the flow direction, decreasing to zero curvature at the throat of the inlet nozzle, is desired. A curve having this property is $r = a\,\theta^{-b}$, where r is the magnitude of a vector $\bar{r}$ with fixed origin O whose direction is specified by the angle θ from a given axis (Vavra (6), page 297). See Figure 13. The constant, a , determines the scale, and the constant, b , specifies the ratio of QP^*/QP_o for a particular δ^* and a prescribed curvature at P_o. The constant, b , cannot be determined explicitly and therefore must be found by interation. Selecting an outer diameter of the larger nozzle ($\beta = 1.0$) twice that of the throat diameter (in this case, the tube or duct diameter); and an outer diameter equal to the tube diameter for the smaller nozzle ($\beta = 0.7$) , the following results are obtained:

	β	Throat Diameter (BP_o) inches	Large Diameter (AP^*) inches	Axial Length (QP_o) inches	$\frac{QP^*}{QP_o}$	b
Small Nozzle	0.7	25.200	36.000	12.500	0.4320	0.6975
Large Nozzle	1.0	36.000	60.000	24.000	0.5000	0.5920

INLET NOZZLE PRESSURE DROP

The ideal pressure drop from the atmosphere at P_a to the throat pressure, p_1' , is given by

$$P_a - p_1' = 1/2\ \rho\ v_1'^{\,2} = q_1'$$

A convenient reference dynamic head, q_{ref} , can be defined in terms of the reference velocity, ωR_m . Recall that the average axial velocity, $\bar{V}_a$, when referred to this reference velocity, is the flow coefficient, $\varphi = \frac{\bar{V}_a}{\omega R_m} = \bar{V}_a^*$. Therefore, let $q_{ref} = 1/2\ \rho_{ref}\ (\omega R_m)^2$ where $\rho_{ref} = \rho_a$. Thus, $q_{ref} = 1/2\ \rho_a\ (\frac{\bar{V}_a}{\varphi})^2$.

Also, any velocity head, q_i , may be expressed in terms of q_{ref} :

$$q_i = q_{ref} \left(\frac{\bar{V}_i}{\bar{V}_a} \right)^2 \varphi^2 \quad \text{where} \quad \rho_i = \rho_a .$$

From the continuity equation: $\dot{m} = \rho_i A_i V_i = \rho_a \pi (R_t^2 - R_h^2) \bar{V}_a$.

If $A_i = \pi R_i^2$, then $q_i = q_{ref} \left[\frac{(R_t^2 - R_h^2)}{R_i^2} \right] \varphi^2$. Note also by definition, $\alpha = \frac{R_h}{R_t}$, and therefore, $(R_t^2 - R_h^2) = R_t^2 (1 - \alpha^2)$.

Hence, $q_i = q_{ref} \frac{R_t^4}{R_i^4} (1 - \alpha^2)^2 \varphi^2$ EQN (23)

Noting that $\frac{A_t}{A_1'} = \frac{R_t^2}{R_1'^2} = \bar{\beta}^2$, $q_1' = \frac{1}{\beta^4} (1 - \alpha^2)^2 q_{ref} \varphi^2$

and thus, $(P_a - P_1')_{ideal} = \frac{1}{\beta^4} (1 - \alpha^2)^2 q_{ref} \varphi^2$.

The actual pressure drop is somewhat greater than this for a given flow rate because of the frictional resistance, and is expressed as

$$(P_a - P_1')_{actual} = (1 - \xi_N)\ (P_a - P_1')_{ideal}$$
$$= (1 - \xi_N)\ \frac{1}{\beta^4}\ (1 - \alpha^2)^2\ q_{ref}\ \phi^2 \qquad \text{EQN (24)}$$

where the loss coefficient, ξ_N , varies from 0.03 to 0.05 depending upon the area ratio. A mean value of 0.04 was selected.

SUDDEN EXPANSION DOWNSTREAM OF INLET NOZZLE

Downstream of the smaller throat diameter inlet nozzle, the flow expands suddenly to the duct tube diameter with a consequent loss in total pressure. Assuming the pressure is constant across the cross-section, the pressure recovery at a cross-section downstream in the tube where the flow has re-established a uniform velocity profile is obtained by applying the momentum equation:

$$P_1' \pi R_t^2 + \dot{m} V_1' = P_E \pi R_t^2 + \dot{m} V_E$$

and the continuity equation:

$$\dot{m} = \rho_1' R_1^2, V_1' = \rho_t R_t^2 V_E .$$

This yields a theoretical static pressure recovery, $\Delta P_{E_{th}}$,

$$\Delta P_{E_{th}} = P_E - P_1' = \frac{\rho_E \pi R_t^2 V_E^2}{\pi R_t^2} - \frac{\rho_1 \pi R_1^2, V_1^2,}{\pi R_t^2}$$

Recalling $\beta = \frac{R_1'}{R_t}$ and $q_i = 1/2\ \rho_i V_i^2$, and assuming incompressible flow,

$$\Delta P_{E_{th}} = 2\ q_1'\ \beta^2\ (1 - \beta^2) \qquad \text{EQN (25)}$$

or, in terms of the reference dynamic head

$$\Delta P_{E_{th}} = 2\ \frac{1}{\beta^2}\ (1 - \beta^2)\ (1 - \alpha^2)^2\ q_{ref}\ \varphi^2 \qquad \text{EQN (26)}$$

Experiments by Souran (7) indicate that the actual pressure recovery, including a tube of a certain length, is somewhat less than the theoretical given by

$$\Delta P_E = (\ 1 - \xi_E\ )\ \Delta P_{E_{th}}$$

where ξ_E varies from 0.03 to 0.05, depending on the area ratio and the length of the tube. The experiments include the frictional pressure drop with the pressure recovery, and therefore the coefficient, ξ_E, includes both effects. Incorporating the frictional pressure drop, ΔP_{T1} equivalent to $P_E - P_2'$, with the sudden expansion yields

$$\Delta P_E - \Delta P_{T1} = P_2' - P_1' = 2\ (1 - \xi_E)\ (\frac{1}{\beta^2} - 1\ )\ (1 - \alpha^2)^2\ q_{ref}\ \varphi^2 \qquad \text{EQN (27)}$$

Two important experimental results of Souran (7) are: first, an almost uniform velocity profile is attained in the tube downstream of the sudden expansion (for an area ratio of 0.5 ($\beta \approx 0.7$), this takes place within about six tube diameters); second, the maximum pressure recovery for an area ratio of 0.5 occurs after about four to five tube diameters. The first result is most important when zero throttling occurs, since throttling as proposed should aid in

the re-establishment of a uniform velocity profile. A uniform velocity profile is required for the input to the compressor and is more important than the maximum pressure recovery possible. Hence, it is concluded that a total length of six tube diameters from the exit of the inlet nozzle to the compressor inlet is desired. The division between upstream and downstream of the throttle will be determined after examining the throttle characteristics.

DOWNSTREAM DUCT LOSS

The pressure drop in the duct tube between the throttle and the compressor inlet is given by

$$\Delta P_{T2} = P_3' - P_4' = \xi_{T2}\, q_{T2}\, \frac{L_2}{2 R_t}$$

where ξ_{T2} is the applicable friction factor. Using Equation (23),

$$\Delta P_{T2} = \xi_{T2}\, \frac{L_2}{2 R_t}\, \left(1 - \alpha^2 \right)^2 q_{ref}\, \varphi^2 \qquad \text{EQN (28)}$$

INLET TO COMPRESSOR

The ideal pressure drop associated with the contraction of the flow area from that of the tube, πR_t^2, to the annular area of the compressor, $\pi (R_t^2 - R_h^2)$, is given by

$$\Delta P_{I_{ideal}} = (P_4' - P_5')_{ideal} = q_5' - q_4'$$

From Equation (23), $q_5' = q_{ref}$; $q_4' = (1 - \alpha^2)^2 \, q_{ref} \, \varphi^2$

Thus,

$$\Delta P_{I_{ideal}} = (1 - (1 - \alpha^2)^2) \, q_{ref} \, \varphi^2$$

The actual pressure drop is greater than the ideal, as represented by

$$\Delta P_{I_{actual}} = P_4' - P_5' = \frac{1}{1 - \xi_I} \Delta P_{I_{ideal}}$$

where ξ_I varies from 0.03 and 0.05. $\xi_I = 0.04$ was selected as a representative average.

Thus, the pressure drop becomes

$$\Delta P_{I_{actual}} = P_4' - P_5' = \frac{1}{1 - \xi_I} (1 - \alpha^2)^2 \, q_{ref} \, \varphi^2 \qquad \text{EQN (29)}$$

INLET AND EXIT GUIDE VANES

The inlet guide vanes for the symmetrical blading were designed to provide the required flow direction, α_1, to the first rotor stage at the design condition. The C-4 circular-arc profile was used. A solidity of 1.0 at the hub varying to about 0.85 at the tip was selected, with a chord varying linearly from hub to tip. The turning angle variation with radius depends not only on the desired flow direction but also on the deviation angle of the flow leaving the guide vane. The method selected for determining this deviation angle is based on the two-dimensional cascade data of Dunavant (8) on a similar six percent maximum profile thickness guide vane, together with the effect of axial velocity variation suggested by Soundranayagain (9). A summary of the design data is given in Table 3.

The exit guide vanes for the symmetrical blading were designed to turn the flow leaving the last stator row back to the axial direction. The radial variation of the inlet flow angles to the exit guide vanes is the same as the outlet flow angles produced by the inlet guide vanes. The maximum turning angle occurs at the outermost or tip radius, R_t . A solidity of approximately 1.2 was selected at the tip, varying to about 1.0 at the hub to provide a margin large enough to avoid flow separation. A linear variation of the blade chord from hub to tip was selected for the exit guide vane using the C-4 circular-arc profile sections. The aerodynamic design followed the method presented in Reference (1). A summary of the design data is given in Table 4. Note that the directional flow changes that occur in the exit guide vanes are equal and opposite to those that occur in the inlet guide vanes. Therefore, neglecting the minor total pressure drops occurring in the guide vanes, the magnitude of the pressure drop in the inlet guide vanes is equal to the magnitude of the pressure recovery in the exit guide vanes.

DIFFUSOR

The ideal pressure recovery in the diffusor at the exit of the compressor is given in terms of the inlet velocity head,

$$q_8' = 1/2 \quad \rho_8' V_8^{2}{}' = 1/2 \quad \rho_a V_a^2$$

and the diffusor area ratio,

$$\frac{A_8'}{A_9'} \quad .$$

$$\Delta P_{D_{ideal}} = (P_9' - P_8')_{ideal} = q_8' \left(1 - \frac{A_8'^2}{A_9'}\right)$$

Note: $A_8' = A_{ref}$ and $q_8' = q_{ref}\ \varphi^2$, therefore,

$$\Delta P_{D_{ideal}} = \left[1 - \left(\frac{A_8'}{A_9'}\right)^2 \right] q_{ref}\ \varphi^2 \qquad \text{EQN (30)}$$

The actual static pressure rise can be defined in one of two ways. First, as a fraction of the ideal pressure rise, that is,

$$\Delta P_{D_{actual}} = \eta_d\ \Delta P_{D_{ideal}}$$

where η_d is the diffusor efficiency. Or, second, as a fraction of the maximum possible pressure recovery. The maximum possible is the recovery of the inlet dynamic head, or equivalently, when A_9 approaches infinity.

$$\Delta P_{D_{actual}} = P_9' - P_8' = \eta_D\ \Delta P_{D_{ideal_{max}}} = \eta_D q_8' = \eta_D\ q_{ref}\ \varphi^2 \qquad \text{EQN (31)}$$

where η_D is the diffusor pressure recovery factor. Note that the two definitions are related to each other by the area ratio term, that is,

$$\eta_D = \left(1 - \left(\frac{A_8'}{A_9'}\right)^2\right) \eta_d$$

The latter method was chosen in order to use the results of Concanover, Kline, and Johnson (10) directly.

A straight-sided, annular, conical diffusor with an area ratio of 1.8 and a length of 2.4 feet was selected. From Reference (10), the recovery factor η_D for the expected range of flow rates is approximately

0.56. (This corresponds to a diffusor efficiency, $\eta_d = 0.81$.) Two other diffusors with shaped contours and with approximately the same area ratio were examined and found to have recovery factors within ten percent of the selected diffusor. Because of the relative simplicity of manufacture, the straight-sided, annular, conical diffusor was selected. Note that the discharge pressure, p_9', is equal to the atmospheric pressure, P_a.

OVERALL PRESSURE COMPATIBILITY

A determination of the operating points for zero or no throttling can now be made with the components selected. The required compressor pressure rise, ΔP_c, is obtained by summation of the actual pressure changes (rises or drops) in the other components of the flow system. Note first that for essentially incompressible flow, the axial velocity components through the compressor remains constant. Thus, the increase in total pressure across the compressor is equal to the increase in static pressure, that is,

$$\Delta P_{t_c} = P_{t_{7'}} - P_{t_{6'}} = P_7' - P_6' = \Delta P_c$$

Therefore, (see Figure 14)

$$\Delta P_c = \Delta P_N - (\Delta P_E - \Delta P_{T1}) + \Delta P_{TH} + \Delta P_{T2} + \Delta P_I + \Delta P_{IGV} - \Delta P_{EGV} - \Delta P_D \qquad \text{EQN (32)}$$

or

$$P_7' - P_6' = (P_a - p_1') - (p_2' - p_1') + (p_2' - p_3') + (p_3' - p_4')$$

$$+ (p_4' - p_5') + (p_5' - p_6') - (p_8' - p_7') - (p_a - p_8')$$

For zero throttling, $\Delta p_{TH} = 0$. Also, $\Delta p_{IGV} = \Delta p_{EGV}$.

Substitution of the previously obtained expressions for the component pressure changes and introducing the previously defined dimensionless pressure rise, $\bar{\pi}_{t_3}$, into Equation (32) yields

$$2 Z \bar{\pi}_{t_3} q_{ref} = q_{ref} \varphi^2 \left[(1 - \xi_N) \frac{(1 - \alpha^2)^2}{\beta^4} - 2(1 - \xi_2)\left(\frac{1}{\beta^2} - 1\right)(1 - \alpha^2)^2 \right.$$

$$\left. + \xi_{T2} \frac{L_2}{2R_t} (1 - \alpha^2)^2 + \frac{1}{(1 - \xi_I)} (1 - (1 - \alpha^2)^2 - \eta_D \right] \qquad \text{EQN (33)}$$

or

$$2 Z \bar{\pi}_{t_3} = \left\{ F \left(\xi_i's, \frac{L_2}{2R_i}, \alpha, \beta, \eta_o \right) \right\} \varphi^2 \qquad \text{EQN (34)}$$

where F is the functional relationship given in explicit form in Equation (33).

Substitution of the previously selected values (summarized here) into Equation (33)

$\xi_N = 0.04$; $\xi_I = 0.04$;

$\xi_E = 0.04$; $\eta_D = 0.56$; $\frac{L_2}{2 R_t} = 3.0$

$\xi_{T2} = 0.02$; $\alpha = 0.6$;

yields for $\beta = 0.7$

$$F = 1.038 \qquad \text{EQN (35)}$$

for $\beta = 1.0$

$$F = 0.506 \qquad \text{EQN (36)}$$

These two expressions are plotted in Figure 15. Plotting the compressor performance on the same figure yields a graphical solution to Equation (34). Also noted on Figure 15 are the design point and stall limit flow functions, .

Operation with one stage of symmetrical blading will be limited to $\varphi \approx 0.95$ which is higher than the design point $\varphi = 0.825$, but about five percent less than the predicted upper stall limit of $\varphi \approx 1.03$. Operation with two stages is possible throughout the complete flow range between the predicted stall limits with an inlet nozzle diameter ratio, $\beta = 1.0$; and for operation with three stages with a $\beta = 0.7$.

Operation with one, two, or three stages of free-vortex or solid-body type blading is possible throughout the expected flow ranges, using an inlet nozzle with a diameter ratio, $\beta = 0.7$.

Thus, the two inlet nozzle geometries selected will be adequate for the expected operating ranges.

THROTTLING DEVICE

From Figure 15, the difference between the compressor pressure curves, $2 Z \bar{\pi}_{t_3}$, and the sum of the losses curves, $F \varphi^2$, represents the pressure loss coefficient required by the throttling device. That is,

$$\left[(1 - \alpha^2)^2 \sum_{i=1}^{n} \xi_{i_{TH}}\right] \varphi^2 = 2 Z \bar{\pi}_{t_3} - F \varphi^2 \qquad \text{EQN (37)}$$

where $\sum_{i=1}^{n} \xi_{i_{TH}}$ is the sum of n throttling elements in series, each having a pressure loss coefficient of $\xi_{i_{TH}}$. This required sum is plotted in Figure 16 as a function of the mass flow function, φ. The flow obstruction throttling elements selected are of two types: screens and performated plates. The elements are circular discs with the same inner diameter as the compressor inlet duct, and are welded to annular rings for rigidity.

The pressure loss coefficients for both type elements were obtained from Reference (11). For screens, a correlation is found relating the pressure loss coefficient to the screen solidity, s , and the flow Reynolds Number based on the approach velocity and the screen wire diameter. The loss coefficient is given by

$$\xi_{TH} = k(Re) \left[1.3\ s + \frac{s^2}{(1 - s)^2} \right]$$

where k(Re) is a function of Reynolds Number and varies between 0.9 and 1.2 for the geometries selected. A summary of the screen configurations selected is given in the table below:

Mesh Number, m ($in.^{-1}$)	4	10	12	12	12
Wire Diameter, d_w (in.)	.028	.016	.018	.025	.028
Solidity, s	.211	.294	.392	.516	.564
Open Area, (1 - s)	.789	.706	.608	.484	.436
Loss Coefficient, ξ_{TH}	.346	.556	.925	1.807	2.407

The material selected for the screen cloth was stainless steel. For perforated plates, it was determined that the feasible combinations of plate thickness, ℓ, hole diameters, d_H, and solidities, s, result in a range of $^{\ell}/_{d_H}$ between 0.2 and 1.0, and a range of Reynolds Numbers (based on velocity through the holes, and the hole diameter,) between 10^4 and 10^5. Within this range of parameters, it has been found that the pressure loss coefficient for a desired plate solidity, $^{\ell}/_{d_H}$ and Re can be related to the pressure loss coefficient for that solidity at reference values of Re = 5×10^4, and $^{\ell}/_{d_H} = 0.4$. That is

$$\xi_{TH}\left(s, Re, \frac{\ell}{d_H}\right) = \xi_{TH}\left(s, Re_o, \left(\frac{\ell}{d_H}\right)_o\right) \cdot K(Re) \cdot K\left(\frac{\ell}{d_H}\right)$$

where $Re_o = 5 \times 10^4$ and $\left(^{\ell}/_{d_H}\right)_o = 0.4$.

A summary of the performated plate configurations selected is given in the table below:

Hole Diameter, d_H (in.)	0.25	0.625	0.750
Hole Spacing, (in.)	0.375	0.875	1.0
Plate Thickness, ℓ (in.)	0.1875	0.1875	0.1875
Solidity, s	0.60	0.54	0.49
Loss Coefficient, ξ_{TH} (at Re_o)	5.26	4.37	3.10

The internal stresses and deformations of the screens and plates selected were also investigated and found to be well within allowable limits. Similarly, the annular support rings were found to be well within allowable limits to support the axial force exerted on the throttling elements.

FINAL ASSEMBLY

Figures 17 through 21 are photographs of the assembled, redesigned compressor facility. Figure 17 is an overall view of that portion of the facility which is housed within the laboratory building. Figure 18 shows the inlet nozzle which is located outdoors. Figure 19 shows the protective netting surrounding the inlet nozzle to minimize the effects of external wind gusts. Figure 20 shows the interchangeable throttling elements, one screen is shown and one perforated plate is shown partially withdrawn through the access door. Figure 21 shows the drive motor, pulley drive, and the torque meter installation.

BIBLIOGRAPHY

1. Vavra, M. H.

Aerodynamic Design of Symmetrical Blading for Three-Stage Axial Flow Compressor Rig, Naval Postgraduate School Report NPS-57VA70091A, Sept. 1970.

2. Lieblein, S.

NASA SP-36, Chapter VI, 1965.

3. Howell, A. R.

Axial Compressor Design, Report E3946, Royal Aircraft Establishment, Farnborough, ENGLAND, June 1942.

4. Bowen, J. T., Sabersky, R. H., and Rannie, W. D.

Investigations of Axial Flow Compressors, Transactions ASME, Jan. 1951, pp. 1-15.

5. Bowen, J. T., Sabersky, R. H., Rannie, W. D.

Theoretical and Experimental Investigations of Axial Flow Compressors, California Institute of Technology, Part 1, January, 1949; Part 2, July, 1949; and Part 3, July 1951.

6. Vavra, M. H.

Aero-Thermodynamics and Flow in Turbomachinery, Wiley, 1960.

7. Souran, G.

Fluid Mechanics of Internal Flow, Proceedings, Elsevier Publishing Co., 1967, Contribution of J. Ackeret, pp. 11, 12.

8. Dunavant, J. C.

Cascade Investigation of a Related Series of Six Percent Thick Guide Vane Profiles and Design Charts, NACA TN3959, 1957.

9. Soundranayagain, S.

Effect of Axial Velocity Variation in Airfoil Cascades, J. Mech. Engrg. Science, 13 (1967), No. 2, pp. 92-99.

10. Cocanover, A. B., Kline, S. J., Johnston, J. P.

A Unified Method for Predicting the Performance of Subsonic Diffusors of Several Geometries, Report TD-10, Thermoscience Division, Dept. of Mechanical Engineering, Stanford University, May, 1965.

11. Idel'chik, I. E.

Handbook of Hydraulic Resistance, Coefficients of Local Resistance and Friction, Israel Program for Scientific Translation, 1966: Translation of Spravochnik po gidrawlicheskim soprotivleniyam, Moscow, 1960.

	Data at Mean Radius, R_m	Vavra Data Ref (1), T.VII	Modified Velocity Triangle Results
ROTOR INLET	$V^*_{a1} = V_{a1/\omega R_m}$	0.8138	0.8250
	V^*_{u1}	0.3171	0.3084
	W^*_{u1}	0.6829	0.6916
	V^*_1	0.8734	0.8807
	W^*_1	1.0624	1.0765
	α_1	21.288	20.496
	β_1	40.0	39.974
	$\Delta V^*_u = V_{a2/\omega W^*_u}$	0.38323	0.38323
ROTOR EXIT	$V^*_{a2} = V_{a2/\omega R_m}$	0.8380	0.8250
	V^*_{u2}	0.7003	0.6916
	W^*_{u2}	0.2997	0.3084
	V^*_2	1.0921	1.0765
	W^*_2	0.8900	0.8807
	α_2	39.886	39.974
	β_2	19.68	20.496

TABLE 1. Comparison of Results of Modified Velocity Triangle with Those of Vavra (1).

β_1' original	30.0	32.0	36.0	40.0	45.0	50.0
modified	29.974	31.974	35.974	39.974	44.974	49.974
$i' - i$	-10.0	-8.0	-4.0	0.0	+5.0	+10.0
i'	-11.828	-9.828	-5.828	-1.828	+3.172	+8.172
$(d\delta/di)_{ref}$	0.060	0.062	0.070	0.078	0.088	0.097
δ	9.79	9.89	11.11	10.39	10.83	11.36
$\Delta\beta'$ original	10.92	12.82	16.60	20.32	24.88	29.35
$\Delta\beta'/\Delta\beta$ "	0.537	0.631	0.817	1.00	1.224	1.444
$\Delta\beta'$ modified	10.46	12.29	15.91	19.478	23.84	28.13
$(i'-i)/\Delta\beta$ mod.	-0.492	-0.394	-0.197	0.0	0.246	0.492
β_2' modified	19.51	19.68	20.06	20.496	21.133	21.85
$V_{a1}^{*'} = V_{a2}^{*'} = \varphi$	1.0520	1.0020	0.9094	0.8250	0.7284	0.6392
ΔV_u^*	0.2339	0.2670	0.3280	0.3832	0.4462	0.5048
$(W_1^*)^2$	1.4749	1.3951	1.2627	1.1589	1.0601	0.9878
$(V_2^*)^2$	1.5001	1.4155	1.2731	1.1589	1.0467	0.9080
$Y'/\bar{Y}$	2.21	1.73	1.14	1.00	1.17	2.26
Y'	0.0625	0.049	0.032	0.028	0.033	0.064
$\bar{\eta}_t'$	0.6025	0.7421	0.8753	0.9144	0.9221	0.8798
$\bar{\pi}_{t3}$	0.1345	0.1891	0.2740	0.3345	0.3927	0.3927
L'/L	0.778	0.846	0.943	1.00	1.028	0.946

TABLE 2. Summary of Off-Design Calculations

$r = R/R_m$		0.75	0.8125	0.875	0.9375	1.0	1.0625	1.125	1.1875	1.25
R	(in.)	10.8	11.7	12.6	13.5	14.4	15.3	16.2	17.1	18.0
chord	(in.)	2.120	2.230	2.340	2.450	2.560	2.670	2.780	2.890	3.000
solidity		1.000	0.971	0.946	0.924	0.905	0.889	0.874	0.861	0.849
max. thickness	(in.)	0.180	0.190	0.200	0.210	0.220	0.230	0.240	0.250	0.260
max. thk/chord		0.0849	0.0852	0.0855	0.0857	0.859	0.0861	0.0863	0.0865	0.867
inlet flow angle, α_1	(°)	0.0	0.0	0.0	0.0	0.0	0.0	0.0	0.0	0.0
outlet flow angle, α_2	(°)	8.468	11.767	14.965	18.122	21.288	24.516	27.857	31.372	35.135
δ	(°)	1.40	2.25	3.15	4.10	5.10	6.15	7.25	8.40	9.60
i	(°)	-0.40	-0.60	-0.80	-1.00	-1.20	-1.40	-1.60	-1.80	-2.00
ϕ	(°)	10.268	14.617	18.915	23.222	27.588	32.066	36.707	41.572	46.735
γ	(°)	-4.734	-6.708	-8.657	-10.611	-12.594	-14.633	-16.754	-18.986	-21.368

TABLE 3. Summary of Inlet Guide Vane Design Data

$r = R/R_m$		0.75	0.8125	0.875	0.9375	1.00	1.0625	1.125	1.1875	1.25
R	(in.)	10.8	11.7	12.6	13.5	14.4	15.3	16.2	17.1	18.0
Chord	(in.)	2.20	2.45	2.70	2.95	3.20	3.45	3.70	3.95	4.20
Solidity		1.037	1.066	1.091	1.113	1.132	1.248	1.163	1.176	1.188
Max. Thickness	(in.)	0.180	0.195	0.210	0.225	0.240	0.255	0.270	0.285	0.300
Max. Thk/Chord		0.0818	0.0796	0.0778	0.0763	0.0750	0.0739	0.0730	0.0722	0.714
Inlet Flow Angle α_1	(°)	8.468	11.767	14.965	18.122	21.288	24.516	27.857	31.372	35.135
Outlet Flow Angle α_2	(°)	0.0	0.0	0.0	0.0	0.0	0.0	0.0	0.0	0.0
δ	(°)	2.868	3.880	4.849	5.806	6.834	7.949	9.189	10.561	12.183
i	(°)	0.154	0.214	0.237	0.205	0.110	-0.081	-0.382	-0.872	-1.604
ϕ	(°)	11.182	15.433	19.577	23.723	28.012	32.546	37.428	42.803	48.922
γ	(°)	2.723	3.837	4.940	6.056	7.172	8.324	9.525	10.841	12.278

TABLE 4. Summary of Exit Guide Vane Design Data.

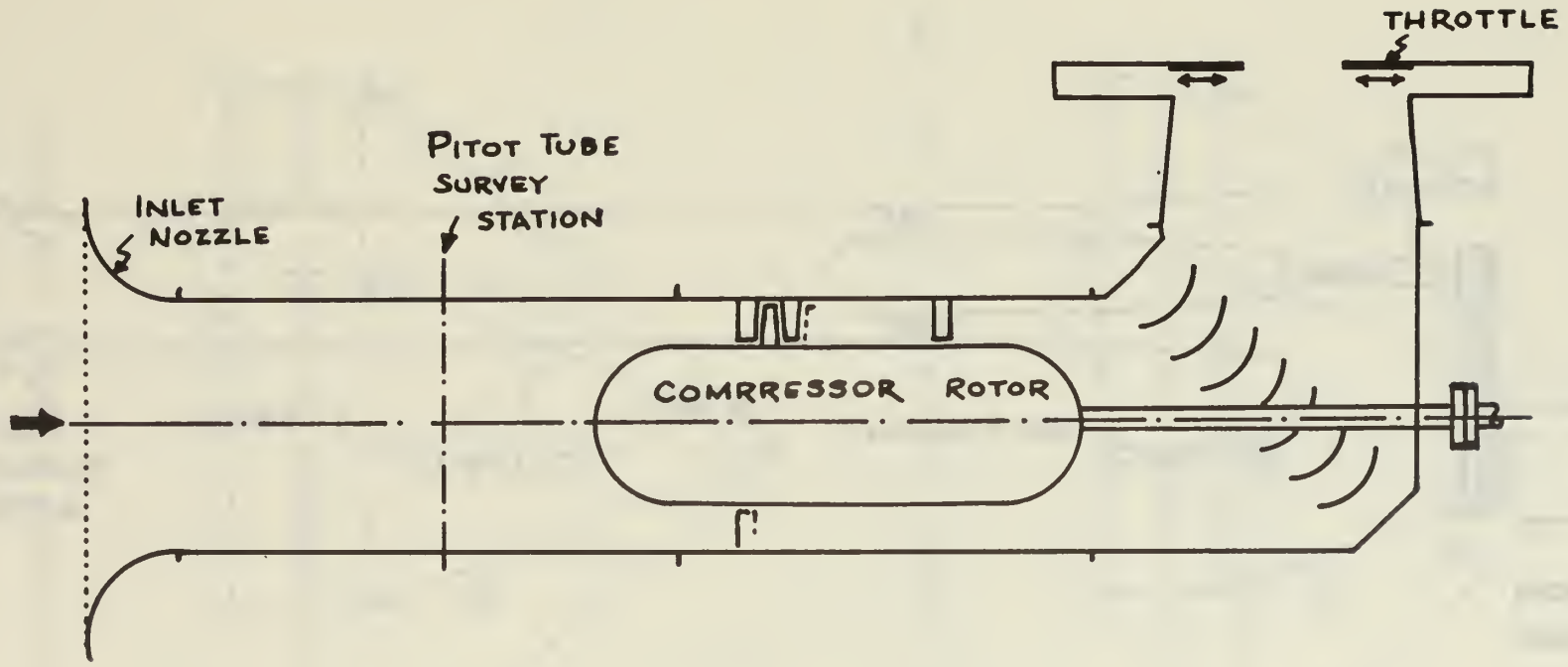

Figure 1. Original Axial Flow Compressor Configuration

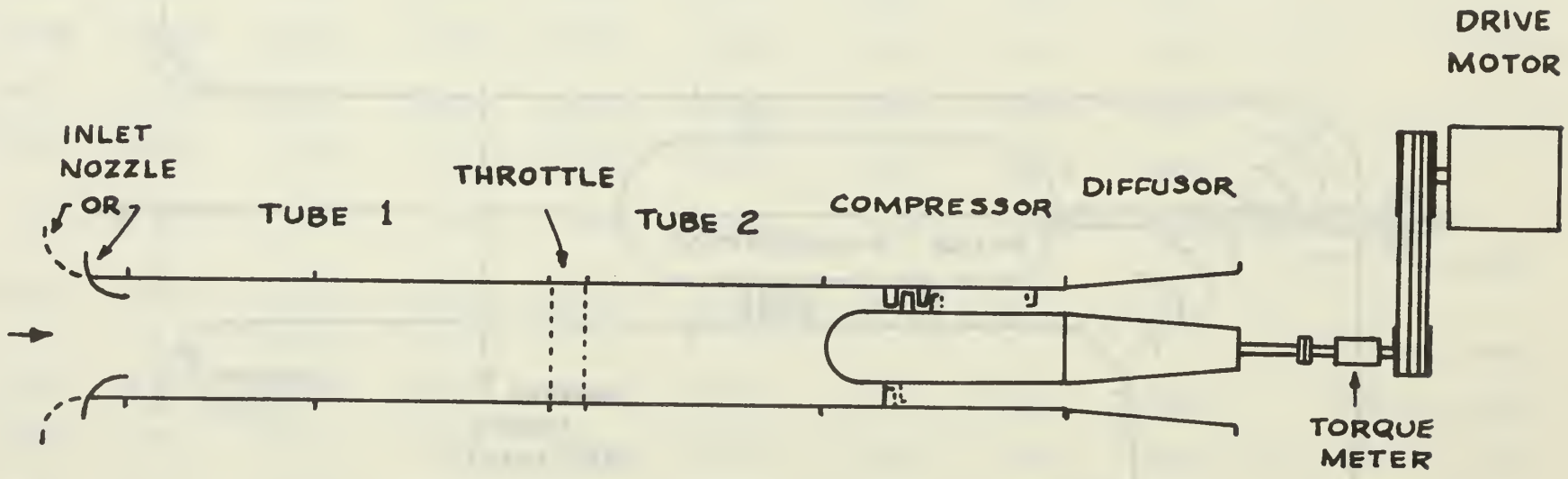

Figure 2. Redesigned Axial Flow Compressor Configuration

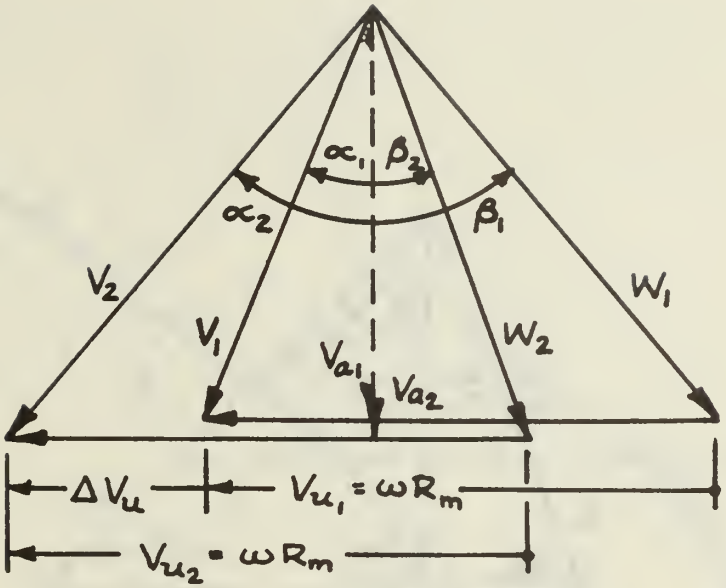

Figure 3(a). Original Velocity Triangle (From Vavra (2))

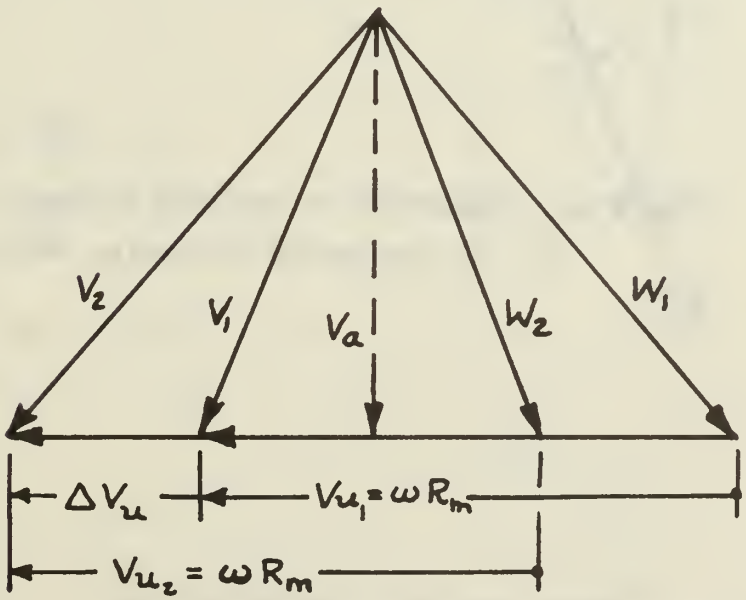

Figure 3(b). Modified Velocity Triangle

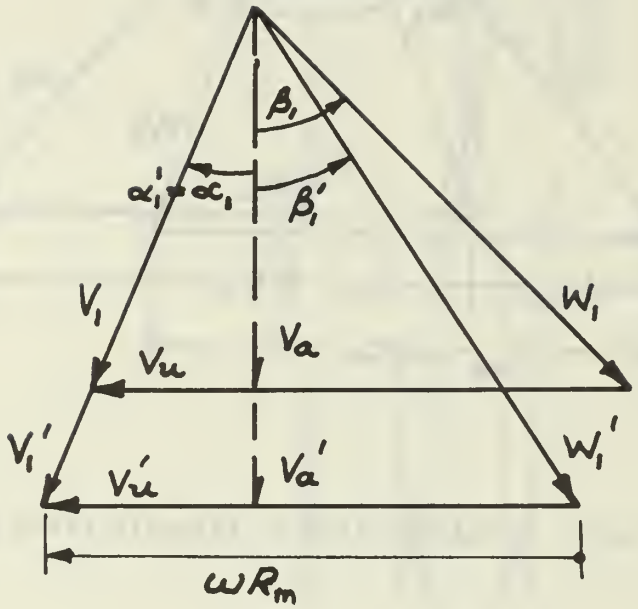

Figure 4. Comparison of Modified Velocity Triangles at Design and Off-Design Conditions

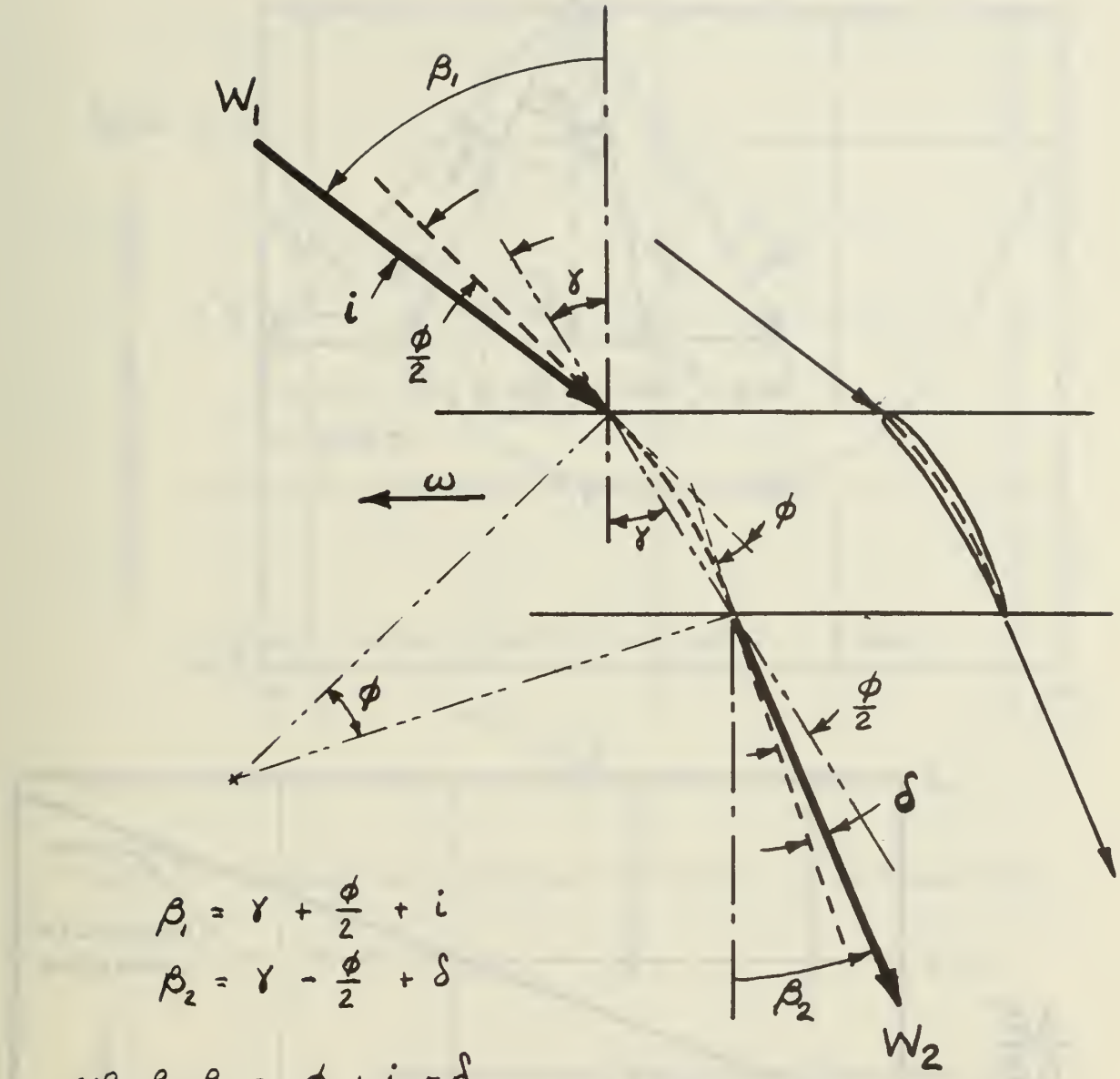

Figure 5. Inter-relationship Between Geometric and Flow Angles for Compressor Rotor Blade

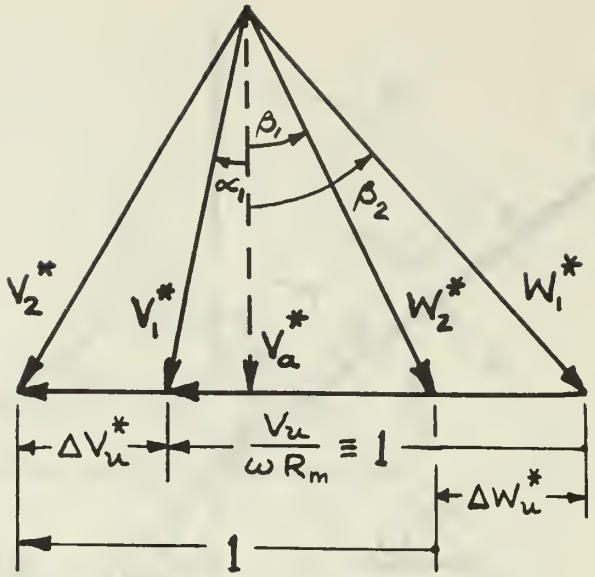

Figure 6. Normalized Modified Velocity Triangle

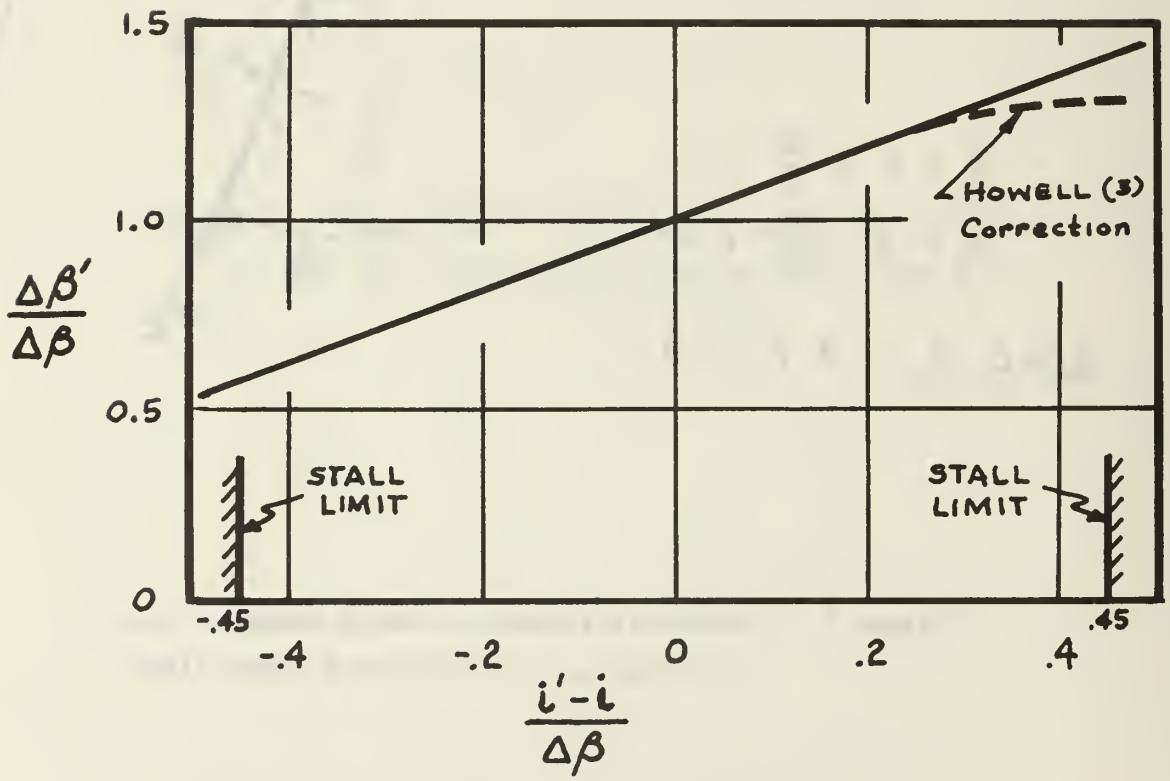

Figure 7. Turning Angle as a function of Incidence Angle

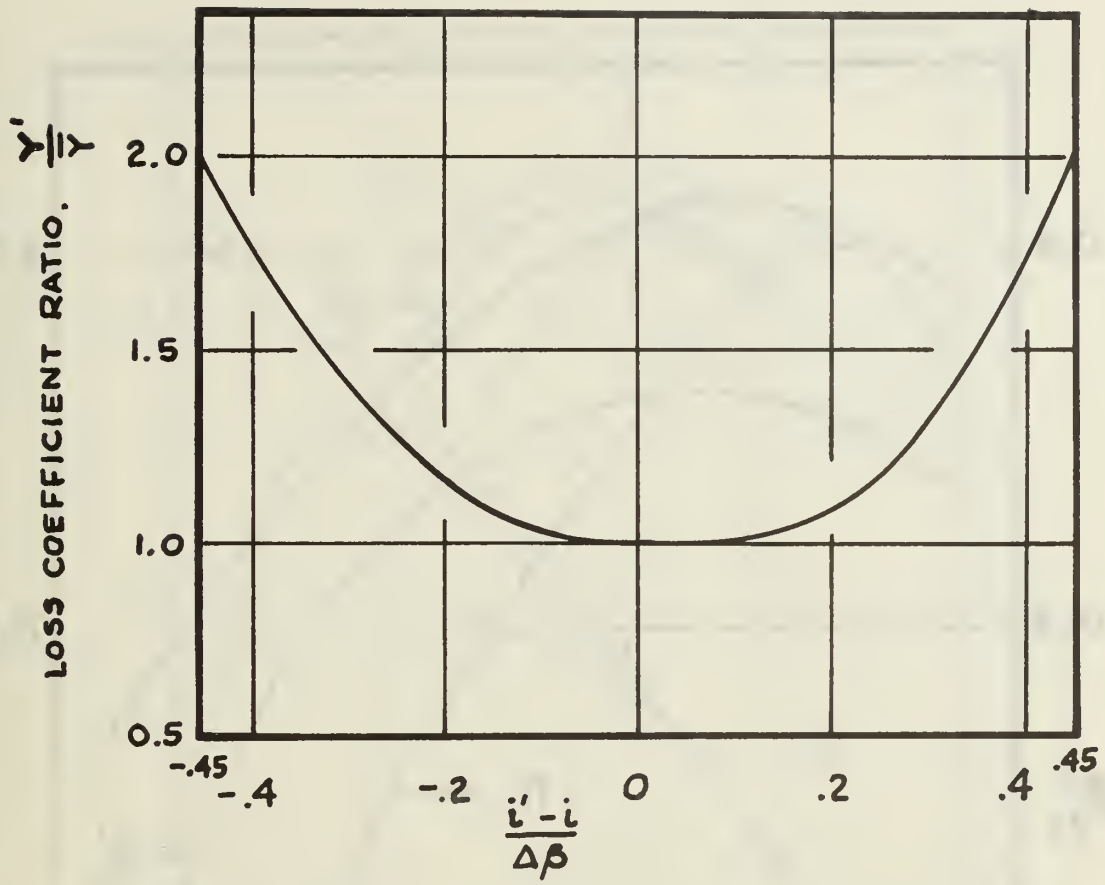

Figure 8. Assumed Loss Coefficient Variation with Incidence Angle

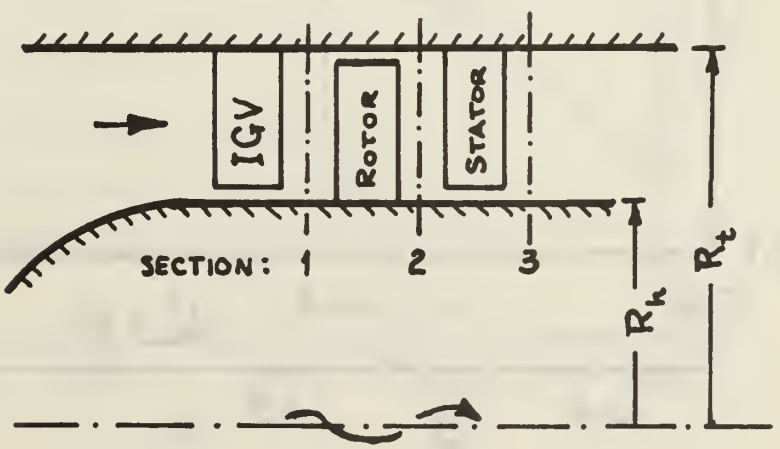

Figure 9. Position Locations within Compressor

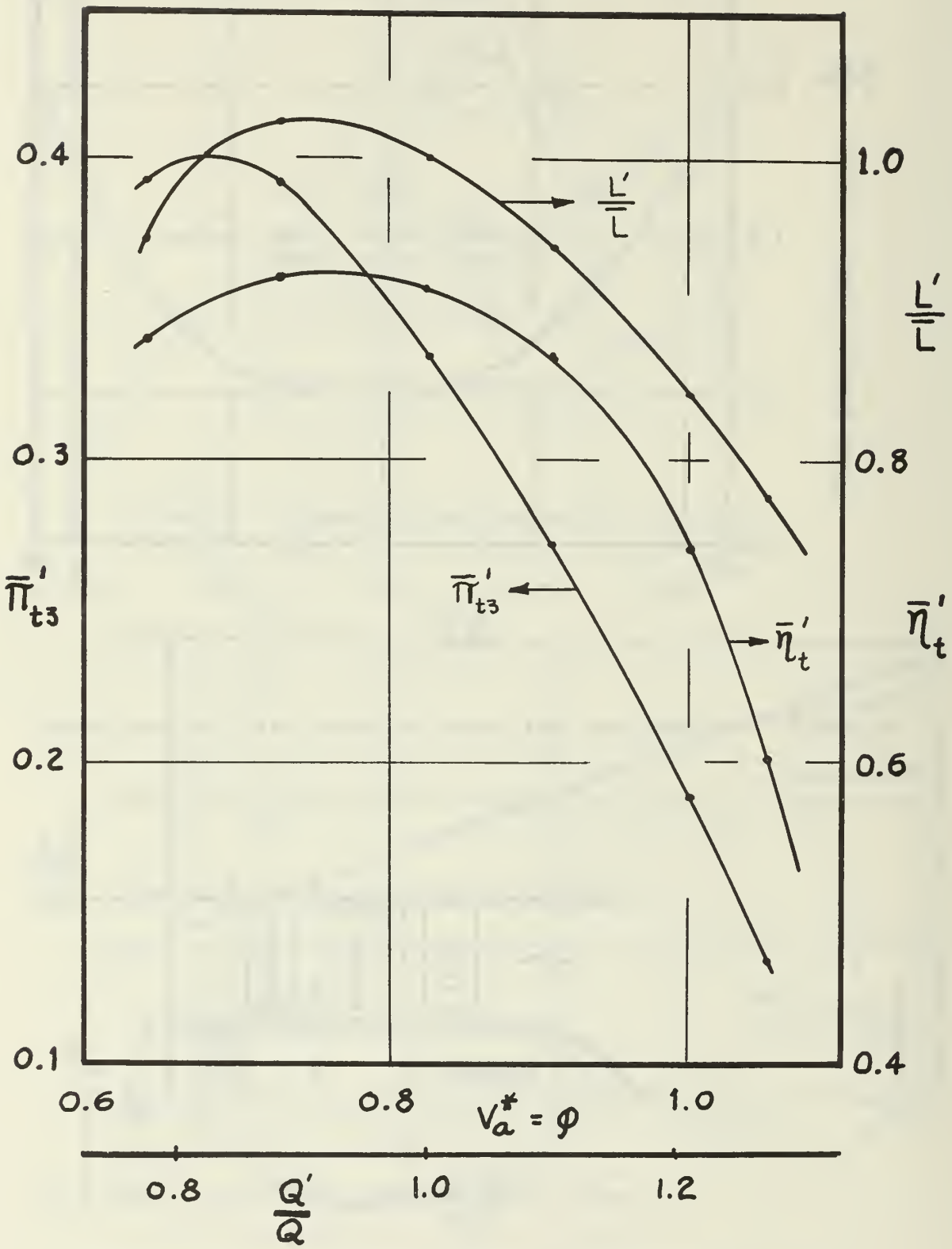

Figure 10. Off-Design Pressure Ratio, Stage Efficiency, and Required Power for the Symmetrical Blading

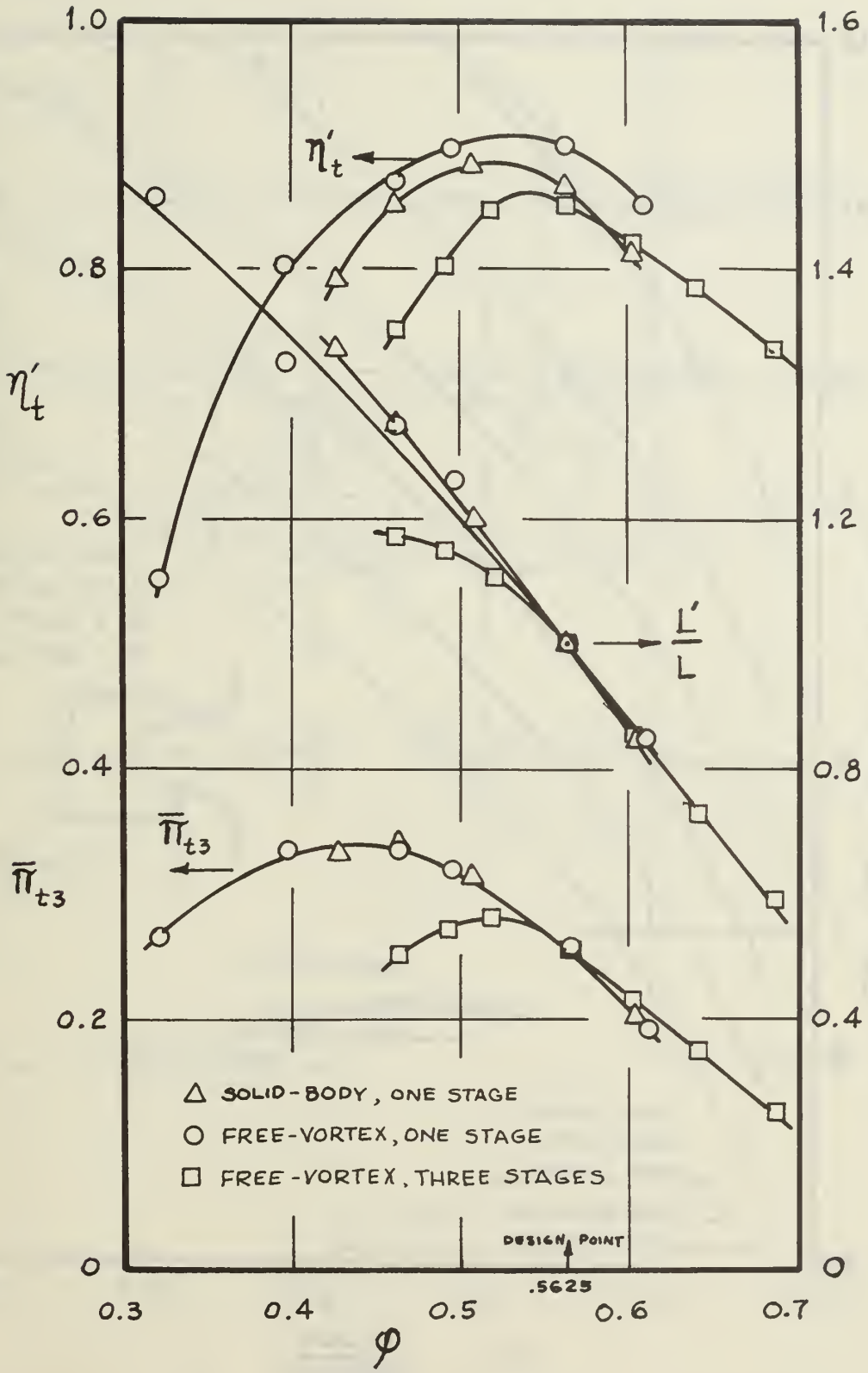

Figure 11. Off-Design Pressure Ratio, Stage Efficiency, and Power Required for the Free-Vortex and Solid-Body type Bladings

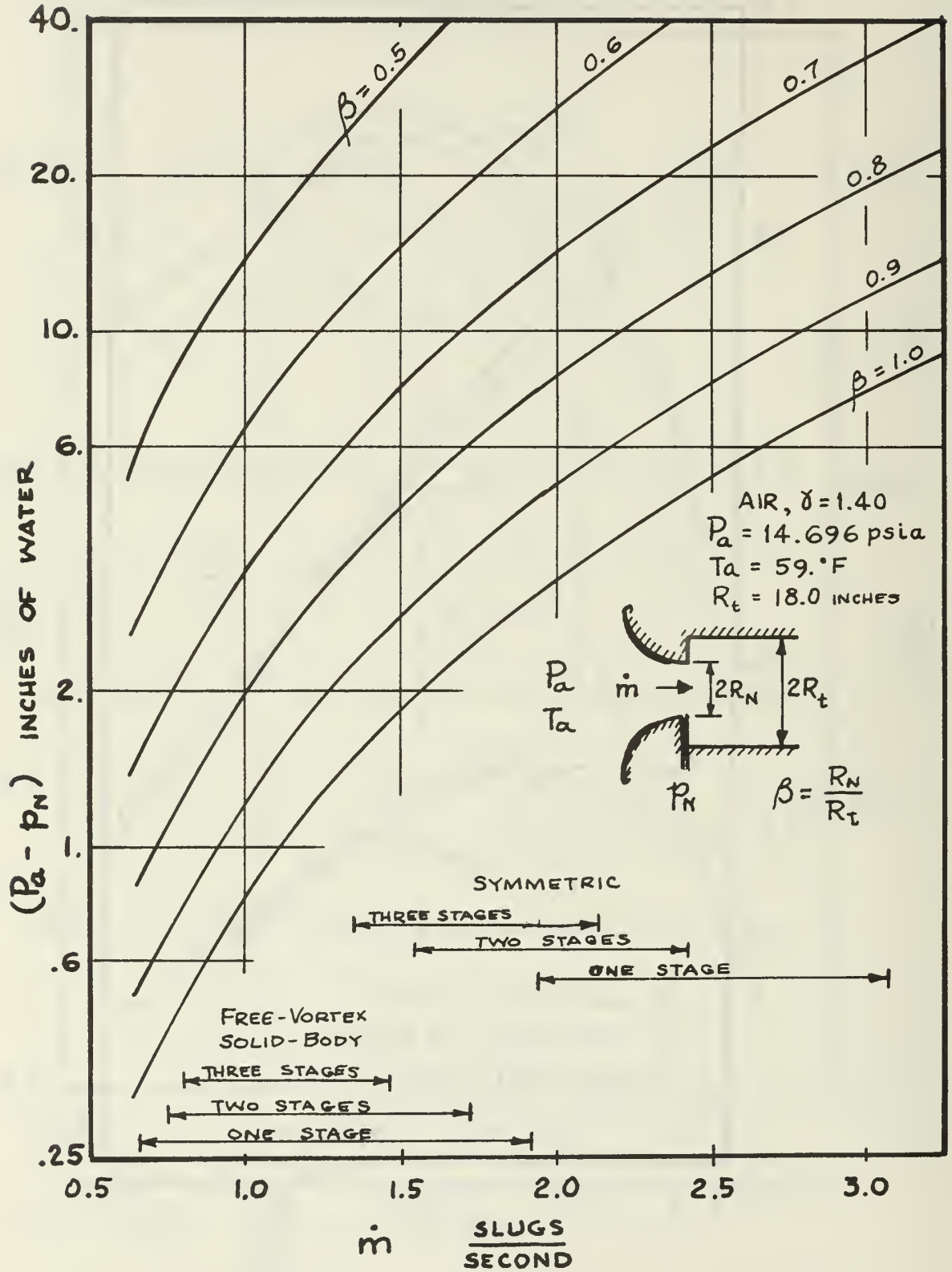

Figure 12. Inlet Nozzle Pressure Drop as a Function of Mass Flow Rate and Nozzle Throat Area

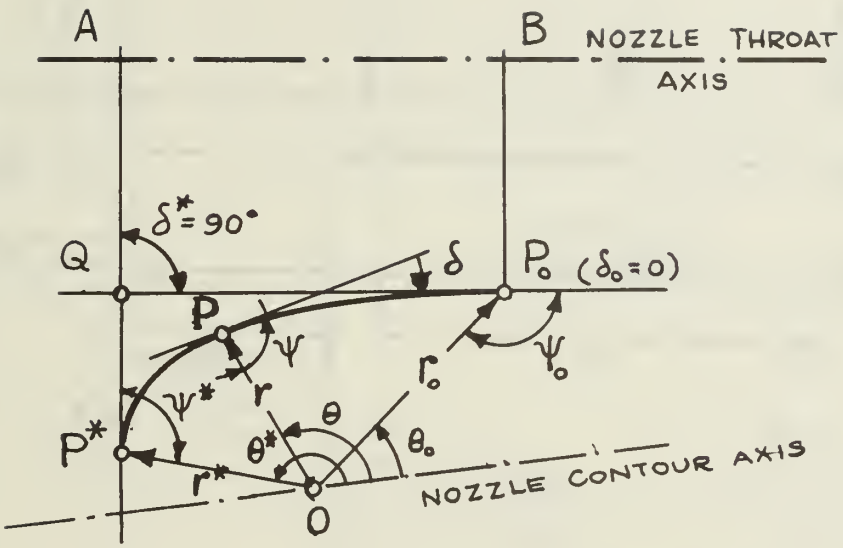

Figure 13. Inlet Nozzle Contour

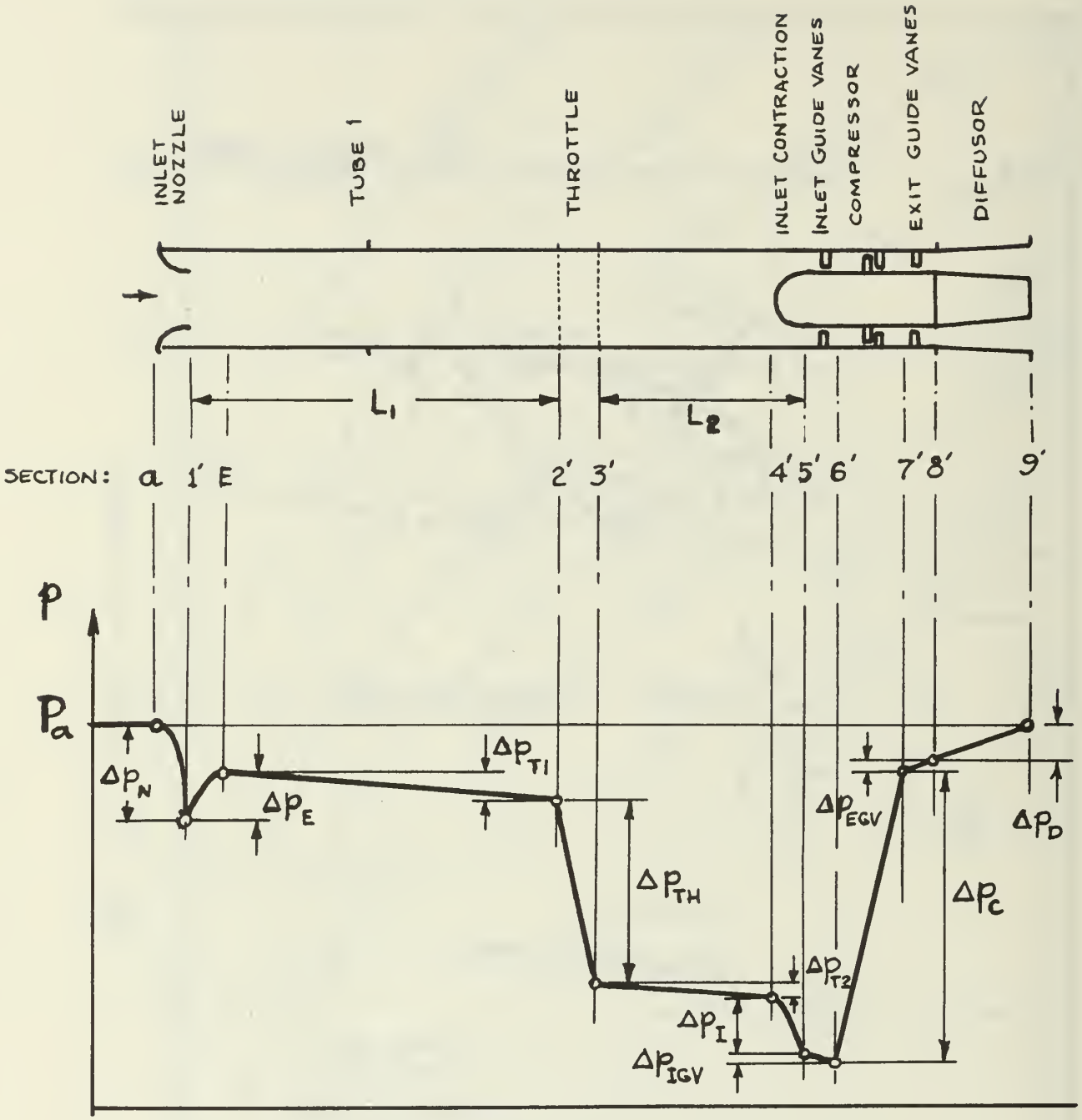

Figure 14. Pressure Variation Through the Compressor Facility

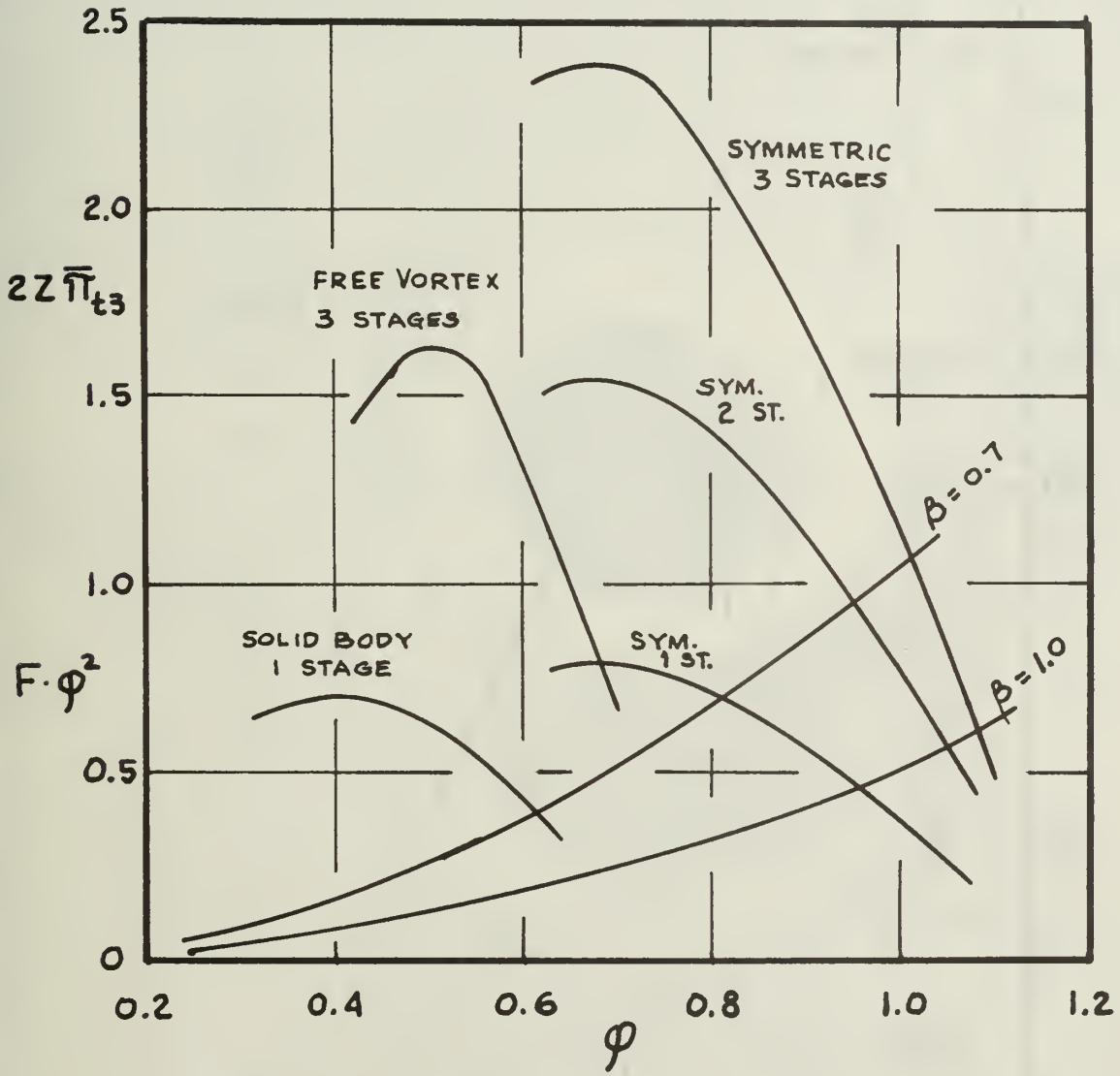

Figure 15. Graphical Solution for Zero Throttling

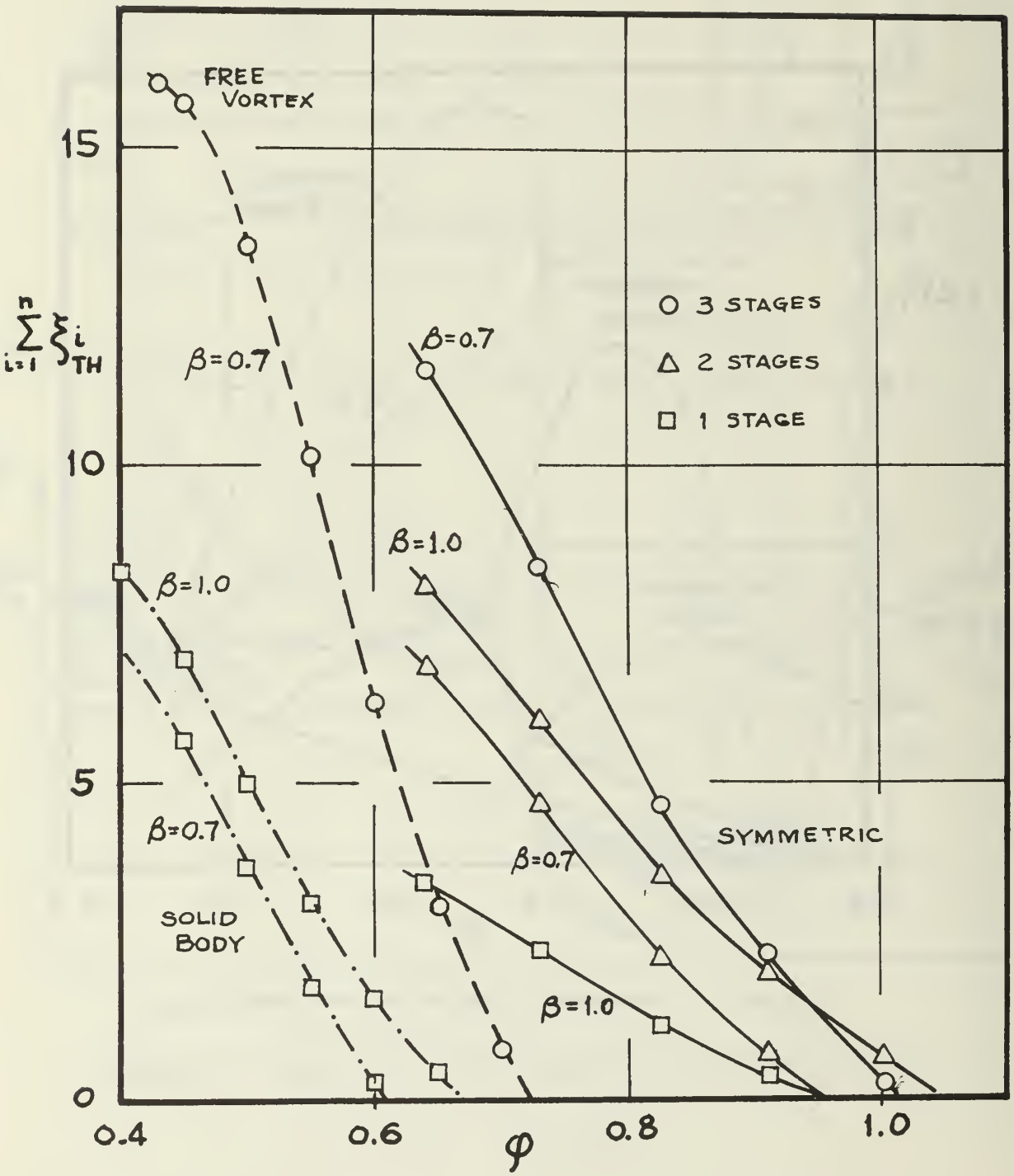

Figure 16. Required Sum of Throttling Element Loss Coefficients

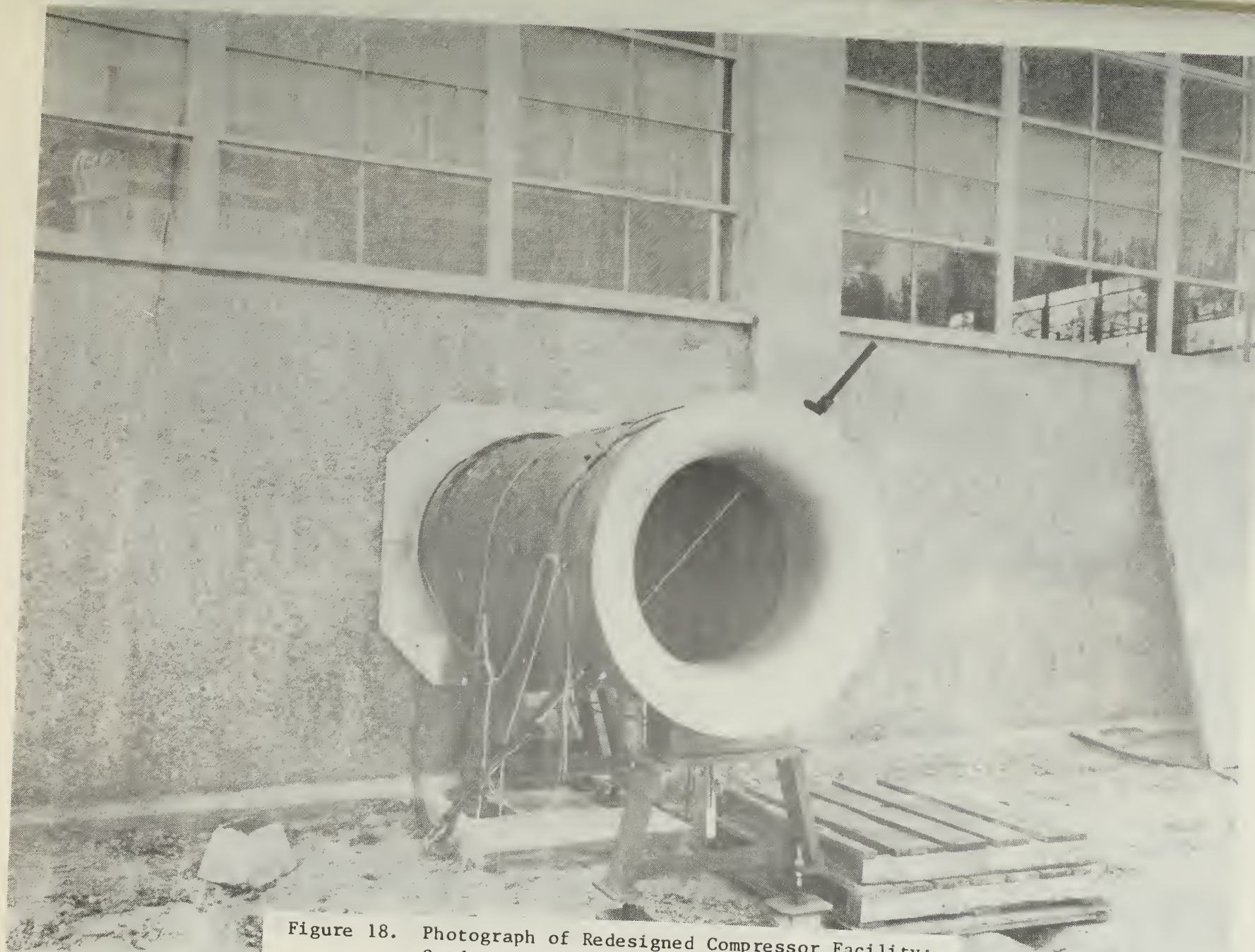

Figure 18. Photograph of Redesigned Compressor Facility: Outdoor Portion Showing Inlet Nozzle

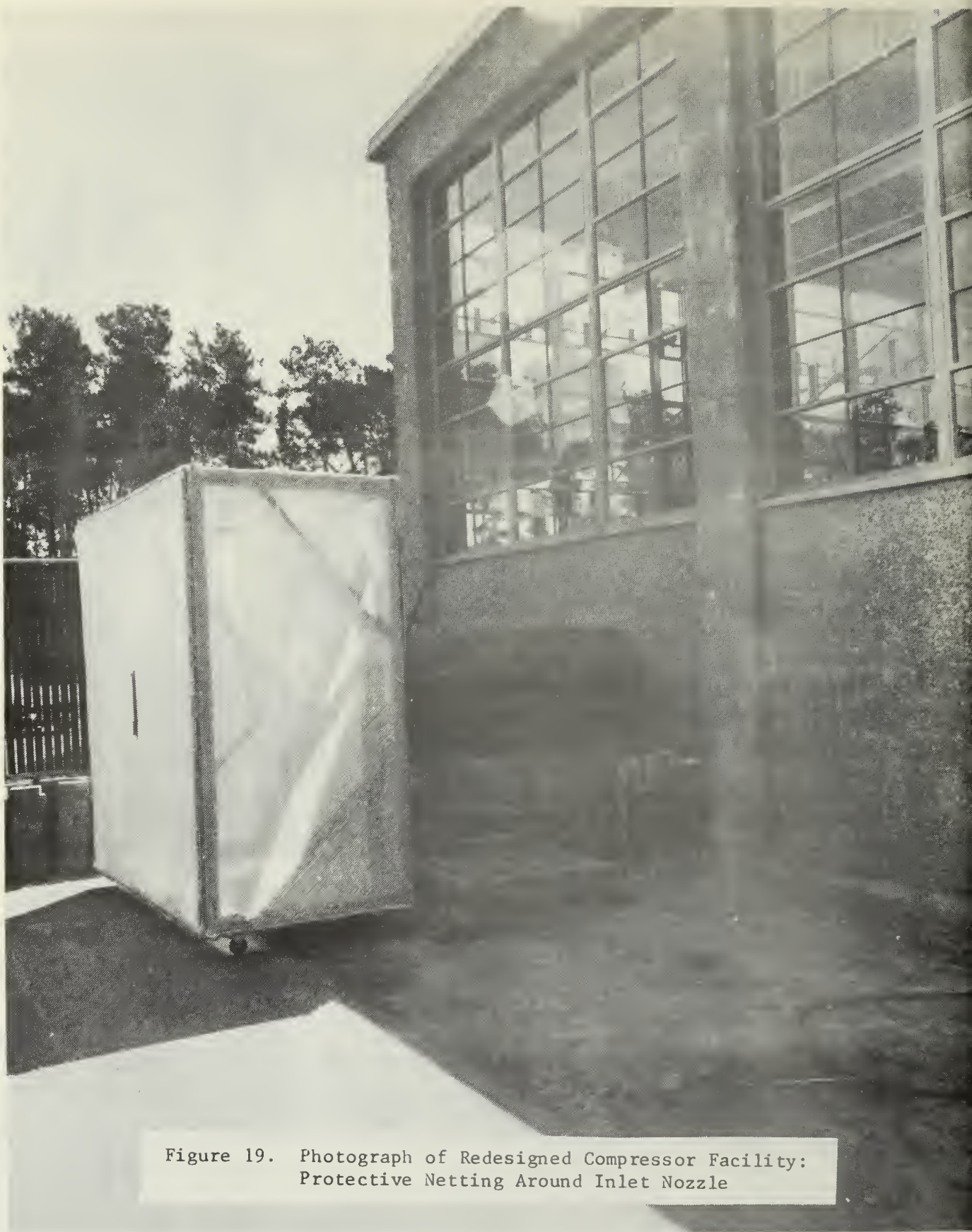

Figure 19. Photograph of Redesigned Compressor Facility: Protective Netting Around Inlet Nozzle

Figure 20. Photograph of Redesigned Compressor Facility: Throttling Elements

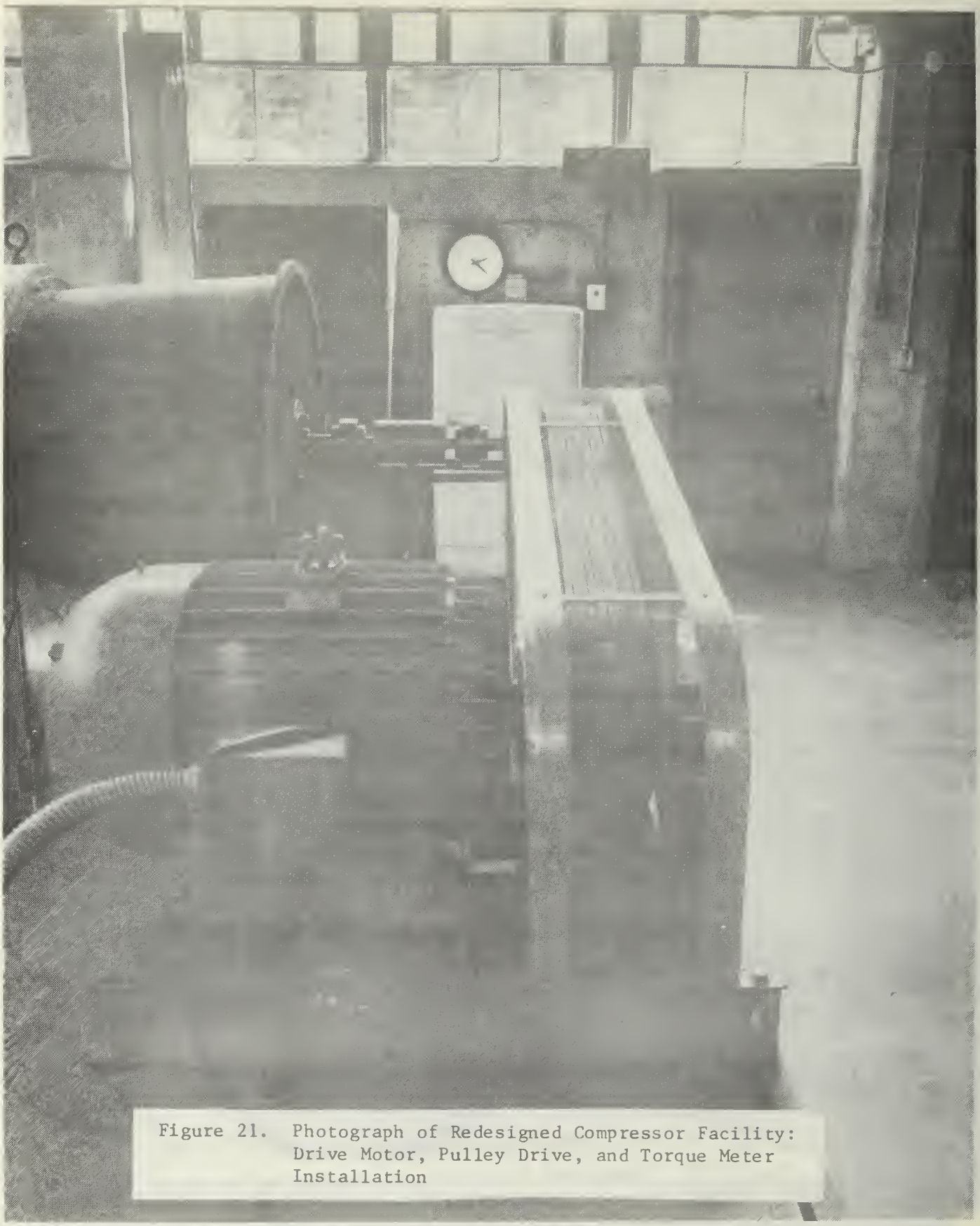

Figure 21. Photograph of Redesigned Compressor Facility: Drive Motor, Pulley Drive, and Torque Meter Installation

APPENDIX A

PROCEDURE FOR OBTAINING THE MODIFIED VELOCITY TRIANGLE AT DESIGN POINT

1. Assume $V_{a_{mod}} = \frac{1}{2}(V_{a_1} + V_{a_2})$; V_{a_1}, V_{a_2} } From Ref (1) TABLE VII

2. $\Delta V_{u_{mod.}} = \Delta V_u$ from Ref. (1) TABLE VII

3.

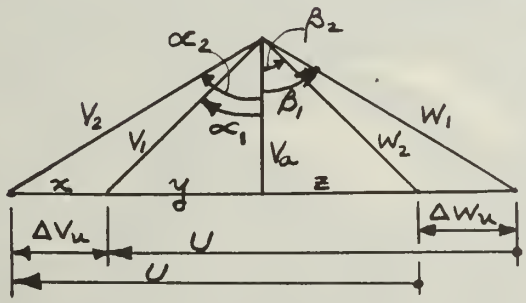

By Symmetry:

$y = z$ $\quad \alpha_1 = \beta_2$

$\Delta V_u = \Delta W_u$ $\quad \alpha_2 = \beta_1$

$$\tan\alpha_1 = \frac{y}{Va} = \frac{\frac{1}{2}(2y)}{Va} = \frac{\frac{1}{2}(U - \Delta V_u)}{Va} = \frac{1}{2}\left(\frac{1 - \frac{\Delta V_u}{U}}{\frac{Va}{U}}\right) = \frac{1 - \Delta V_u^*}{V_a^*}$$

SOLVE FOR α_1

$$\tan\beta_1 = \frac{x+y}{Va} = \frac{U-y}{Va} = \frac{U}{Va} - \frac{y}{Va} = \frac{1}{V_a^*} - \tan\alpha_1$$

SOLVE FOR β_1

4. $\Delta\beta_{mod} = \beta_2 - \beta_1$

5. $V_1 = \frac{Va}{\cos\alpha_1}$; $V_2 = \frac{Va}{\cos\alpha_2}$; $W_1 = V_2$; $W_2 = V_1$

$V_{u_1} = Va \tan\alpha_1$

$W_{u_1} = Va \tan\beta_1$ also $W_{u_1} = U - V_{u_1}$

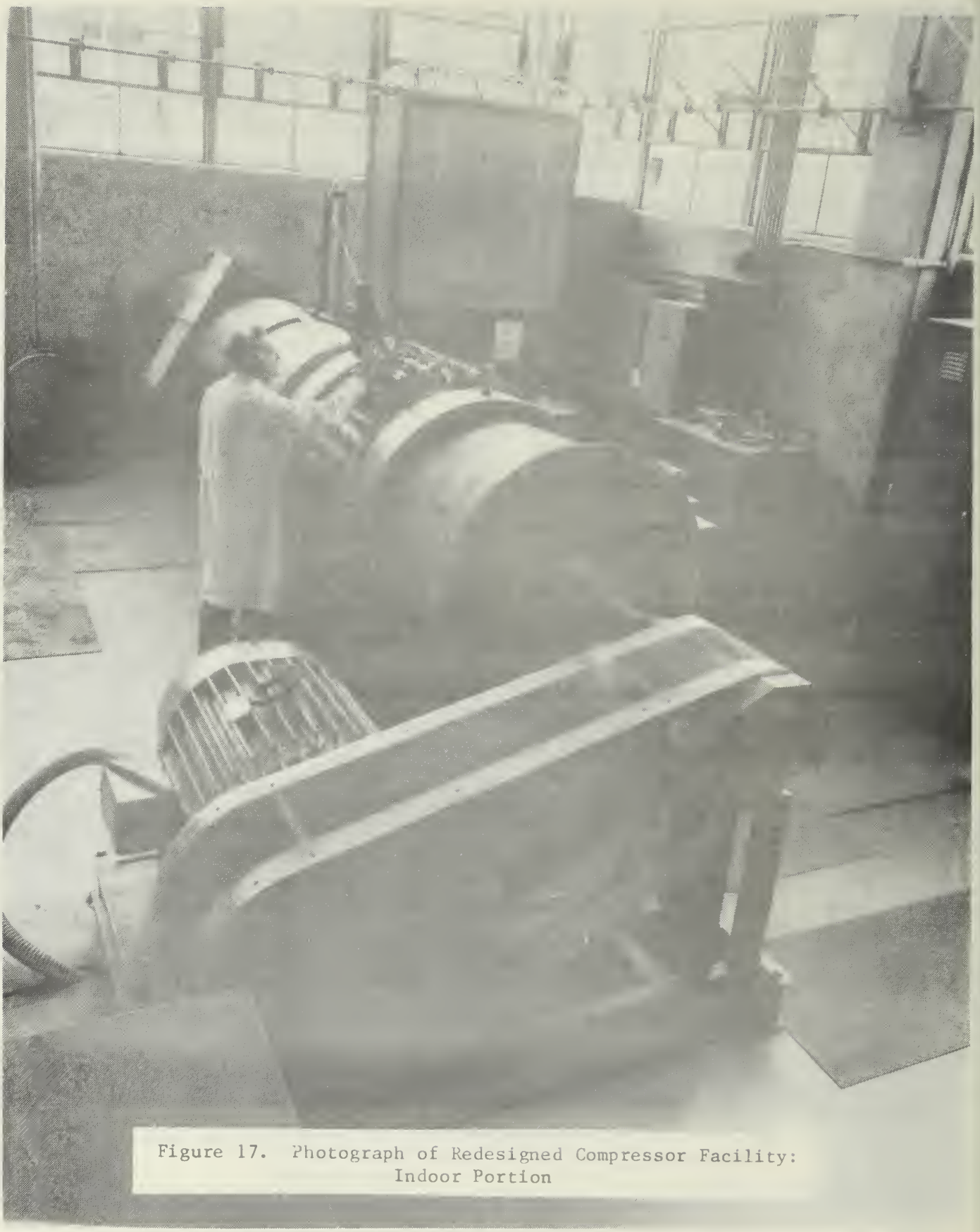

Figure 17. Photograph of Redesigned Compressor Facility: Indoor Portion

DISTRIBUTION LIST

		No. of Copies
1.	Defense Documentation Center Cameron Station Alexandria, Virginia 22314	12
2.	Library Code 0212 Naval Postgraduate School Monterey, California 93940	2
3.	Superintendent Code 00 Naval Postgraduate School Monterey, California 93940	1
4.	Provost Code 02 Naval Postgraduate School Monterey, California 93940	1
5.	Dean of Research Code 023 Naval Postgraduate School Monterey, California 93940	1
6.	Chairman Department of Aeronautics Code 57 Naval Postgraduate School Monterey, California 93940	1
7.	Chairman Department of Mechanical Engineering Code 59 Naval Postgraduate School Monterey, California 93940	1
8.	Turbo-Propulsion Laboratory Department of Aeronautics Naval Postgraduate School Monterey, California 93940	5
9.	Commanding Officer Naval Air Systems Command Navy Department Washington, D. C. 20360	1
10.	Dr. H. J. Mueller Research Administrator Code 310A Naval Air Systems Command Navy Department Washington, D. C. 20360	2

11. Mr. E. A. Lichtman
Naval Air Systems Command
Code 330
Navy Department
Washington, D. C. 20360 — 1

12. Mr. Karl H. Guttman
Code 330C
Naval Air Systems Command
Navy Department
Washington, D. C. 20360 — 1

13. Acquisition Inf
Code AIR - 50174 — 14

14. Rear Admiral C. O. Holmquist, USN
Chief of Naval Research
Office of Naval Research
Arlington, Virginia 22218 — 1

15. Commanding Officer
Naval Air Propulsion Test Center
Attn: Mr. E. Stawski
Trenton, New Jersey 08628 — 1

16. Mr. Eric Lister
R & T Division
Naval Air Propulsion Test Center
Trenton, New Jersey 08628 — 1

17. National Aeronautics and Space Administration
Lewis Research Center (Library)
2100 Brookpark Road
Cleveland, Ohio 44135 — 1

18. Library
General Electric Company
Aircraft Engine Technology Division
DTO Mail Drop H43
Cincinnati, Ohio 45215 — 1

19. Library
Pratt and Whitney Aircraft
Post Office Box 2691
West Palm Beach, Florida 33402 — 1

20. Library
Pratt and Whitney Aircraft
East Hartford, Connecticut 06108 — 1

21. Prof. Paul F. Pucci
Code 59 Pc
Naval Postgraduate School
Monterey, California 93940 — 1

22. Dr. W. Schlachter
Brown, Boveri-Sulzer Turbomachinery Ltd
Dept. TDE
Escher Wyss Platz
CH-8023 Zurich
Switzerland 1

23. Dr. George K. Serovy
Professor of Mechanical Engineering
208 Mechanical Engineering Building
Iowa State University
Ames, Iowa 50010 1

UNCLASSIFIED

SECURITY CLASSIFICATION OF THIS PAGE (When Data Entered)

REPORT DOCUMENTATION PAGE

READ INSTRUCTIONS BEFORE COMPLETING FORM

1. REPORT NUMBER: NPS57VA73121A	2. GOVT ACCESSION NO.
3. RECIPIENT'S CATALOG NUMBER	
4. TITLE (and Subtitle): REDESIGN OF THE LOW SPEED THREE STAGE AXIAL FLOW COMPRESSOR TEST FACILITY	5. TYPE OF REPORT & PERIOD COVERED: Progress Report to July 1973
	6. PERFORMING ORG. REPORT NUMBER
7. AUTHOR(s): M. H. Vavra, P. F. Pucci, W. Schlachter	8. CONTRACT OR GRANT NUMBER(s): Air Task No. A310310A/186A/3R02403001 Ref. b
9. PERFORMING ORGANIZATION NAME AND ADDRESS: Department of Aeronautics, Naval Postgraduate School, Monterey, CA 93940	10. PROGRAM ELEMENT, PROJECT, TASK AREA & WORK UNIT NUMBERS: N/A
11. CONTROLLING OFFICE NAME AND ADDRESS: Naval Air Systems Command, AIR - 310	12. REPORT DATE: December 1973
	13. NUMBER OF PAGES: 60
14. MONITORING AGENCY NAME & ADDRESS (if different from Controlling Office)	15. SECURITY CLASS. (of this report): Unclassified
	15a. DECLASSIFICATION/DOWNGRADING SCHEDULE

16. DISTRIBUTION STATEMENT (of this Report)

Approved for public release, distribution unlimited

17. DISTRIBUTION STATEMENT (of the abstract entered in Block 20, if different from Report)

18. SUPPLEMENTARY NOTES

19. KEY WORDS (Continue on reverse side if necessary and identify by block number)

Axial Compressor Test Rig
Inlet Throttle
Flow Measuring Nozzles

20. ABSTRACT (Continue on reverse side if necessary and identify by block number)

A flow configuration of an existing low-speed, axial flow compressor test facility at the Turbopropulsion Laboratory, Naval Postgraduate School, Monterey, California, was redesigned in order to improve compressor inlet velocity distribution, improve mass flow measurement, and increase the power input. The design of the new configuration, consisting of an inlet nozzle, ducting, throttling device upstream of the compressor, and a diffusor downstream of it, is reported. The redesign is based on using the existing free-vortex type and solid-body type bladings, and the newly designed symmetrical blading.

DD FORM 1 JAN 73 1473 EDITION OF 1 NOV 65 IS OBSOLETE
S/N 0102-014-6601 |
(Page 1)

UNCLASSIFIED
SECURITY CLASSIFICATION OF THIS PAGE (When Data Entered)